

# Krylov localization as a probe for ergodicity breaking

Heiko Georg Menzler<sup>1,\*</sup> and Rishabh Jha<sup>1,†</sup>

<sup>1</sup>*Institute for Theoretical Physics, Georg-August-Universität Göttingen,  
Friedrich-Hund-Platz 1, 37077 Göttingen, Germany*

Krylov complexity has recently gained attention where the growth of operator complexity in time is measured in terms of the off-diagonal operator Lanczos coefficients. The operator Lanczos algorithm reduces the problem of complexity growth to a single-particle semi-infinite tight-binding chain (known as the Krylov chain). Employing the phenomenon of Anderson localization, we propose the inverse localization length on the Krylov chain as a probe to detect weak ergodicity-breaking. On the Krylov chain we find delocalization in an ergodic regime, as we show for the SYK model, and localization in case of a weakly ergodicity-broken regime. Considering the dynamics beyond scrambling, we find a collapse across different system sizes at the point of weak ergodicity-breaking leading to a quantitative prediction. We further show universal traits of different operators in the ergodic regime beyond the scrambling dynamics. We test for two settings: (1) the coupled SYK model, and (2) the quantum East model. Our findings open avenues for mapping ergodicity/weak ergodicity-breaking transitions to delocalization/localization phenomenology on the Krylov chain.

*Introduction.*— As Landau and Lifshitz remarked years ago [1], “According to the fundamental principles of statistical physics, the result of statistical averaging does not depend on whether it is with respect to the exact wave function of a stationary state of a closed system or by means of the Gibbs distribution.” Thermalization in closed quantum systems has long been a topic of deep interest and has led to a wide variety of concepts such as ergodicity, quantum chaos and integrability. The modern cornerstone, namely the Eigenstate Thermalization Hypothesis (ETH), was established in a series of papers [2–7] and is generally taken as the defining feature of quantum ergodicity [8–11]. A prerequisite for quantum thermalization is quantum ergodicity that fundamentally relates to the concept of quantum chaos. However, the two are not the same as has been recently highlighted in [12] where a metric has been proposed for quantum states to differentiate between integrability, chaos and ergodicity. Recently, the “universal operator growth hypothesis” (UOGH) [13] has provided a way of detecting quantum chaos and operator complexity via the so-called *Krylov complexity* (K-complexity). K-complexity has been extensively studied in a variety of systems ranging from many-body localized systems and non-local spin chains to open quantum systems as well as relativistic systems [14–34]. However, as was shown in [19], the UOGH can still be satisfied by some (non-chaotic) integrable systems, highlighting the difference between chaos and scrambling. The exponential growth of out-of-time correlator (OTOC) is considered to be a hallmark probe for quantum chaos but it also grows exponentially for integrable semi-classical systems due to the presence of unstable saddle points [35, 36]. Therefore there exists a hierarchy in the conceptual foundation of thermalization of closed quantum systems, namely

among ergodicity, quantum chaos, scrambling and integrability. Any deviation from the ETH implies weak ergodicity-breaking where there either exists some non-thermal eigenstates and/or admits slow relaxation dynamics from some initial conditions. For example, in the context of adiabatic gauge potential (AGP) [37], when the ETH scaling fails, the system either admits delayed thermalization [38] or does not thermalize at all while being chaotic [12]. Other examples include quantum scars and Hilbert space fragmentation that can also lead to weak ergodicity-breaking [39–45]. In this work, we present a probe to investigate the weak breaking of quantum ergodicity in terms of complexity of arbitrary operators and map the problem of ergodic/weak ergodicity-breaking transitions to delocalization/localization phenomenology on the Krylov chain. We showcase this for the Sachdev-Ye-Kitaev model (SYK) [46–49] that has gained attraction for its analytical tractability despite being a non-integrable and chaotic system.

The other system we consider is the quantum East model [50, 51] which—in contrast to the coupled SYK model—has a local structure and shows at least weakly ergodicity-broken dynamics without the use of disorder [52, 53]. The quantum East model was first introduced in the context of many-body localization (MBL) as an exemplary model that showed indicators for localization without disorder [50, 54] because the mechanism for weak ergodicity-breaking in the quantum East model is based on kinetic constraints [52, 53]. Hence, there exists a natural connection to other systems that show slow thermalization [55] and systems with quantum scars [41, 56]. Recent studies have also shown how quantum East models with particle number conservation are connected to systems observing Hilbert space fragmentation [39, 40, 57].

We compare both models at infinite temperature with previous studies [38, 52] and we find that delocalization/localization on the Krylov chain captures the onset of weak ergodicity-breaking.

*Formal Setting.*— We consider a vector space of bounded operators in the Hilbert space  $\mathbf{H}$  (of dimen-

\* [heiko.menzler@uni-goettingen.de](mailto:heiko.menzler@uni-goettingen.de)

† [rishabh.jha@uni-goettingen.de](mailto:rishabh.jha@uni-goettingen.de)

sion  $\mathcal{N}$ ) denoted by  $\mathcal{B}(\mathbf{H})$  where  $\dim(\mathcal{B}(\mathbf{H})) = \mathcal{N}^2$ . Krylov complexity is defined in terms of Heisenberg evolution of any initial operator  $\mathcal{O}_0$  belonging to  $\mathcal{B}(\mathbf{H})$  corresponding to a given Hamiltonian  $\mathcal{H}$ . Hence it is easier to use the operator-to-state mapping  $\mathcal{O} \rightarrow |\mathcal{O}\rangle$  where the action of the Liouvillian operator  $\mathcal{L} \equiv i[\mathcal{H}, \bullet]$  leads to time evolution given by  $|\mathcal{O}(t)\rangle = \sum_{n=0}^{\infty} \frac{t^n}{n!} |\mathcal{L}^n \mathcal{O}_0\rangle$  [58]. The recursive application of  $\mathcal{L}$  on  $|\mathcal{O}_0\rangle$  generates a Krylov space of operators where we apply the Lanczos algorithm to find the Krylov basis [59]. This requires defining an inner-product in  $\mathcal{B}(\mathbf{H})$  where we chose the Wightman inner-product given by  $(A|B) = \langle e^{-\beta\mathcal{H}/2} A^\dagger e^{-\beta\mathcal{H}/2} B \rangle_\beta$ , where  $\beta$  is the inverse temperature. Since we investigate the infinite temperature case in this paper, this boils down to  $(A|B) = \frac{1}{\mathcal{N}} \text{Tr}[A^\dagger B]$ . We generate a set of ortho-normalized basis vectors  $\{|\mathcal{O}_n\rangle\}_{n=0}^{\mathcal{K}-1}$  where  $\mathcal{K}$  is the dimension of the Krylov space bounded from above by  $\mathcal{K} \leq \mathcal{N}^2 - \mathcal{N} + 1$  [18]. The Lanczos algorithm allows for a matrix representation for the Liouvillian operator  $\mathcal{L}$  in a tri-diagonal form where the off-diagonal elements are given by the Lanczos coefficients  $\{b_n\}_{n=1}^{\mathcal{K}-1}$  (diagonal elements are vanishing). Details of the algorithm and the associated numerical instabilities can be found in the supplemental material.

We can now expand any operator in the Krylov space as  $|\mathcal{O}(t)\rangle = \sum_{n=0}^{\mathcal{K}-1} \phi_n(t) |\mathcal{O}_n\rangle$  where we have  $|\mathcal{O}(t=0)\rangle = |\mathcal{O}_0\rangle$ . The time-dependent coefficients  $\phi_n(t)$  capture the spread of the operator over different Krylov basis vectors. Using the Heisenberg equation of motion, it can be shown (derived in the supplemental material) that  $\phi_n(t)$  satisfies the “real-wave-equation-type” differential equation [60]:  $\partial_t \phi_n(t) = b_n \phi_{n-1}(t) + b_{n+1} \phi_{n+1}(t)$  with the initial conditions  $\phi_n(t=0) = \delta_{n,0}$ ,  $b_{n=0} = 0$  and  $\phi_{-1}(t) = 0$ . Therefore solving for  $\phi_n(t)$  is equivalent to evolving the operator. Thus, the Lanczos coefficients  $\{b_n\}_{n=1}^{\mathcal{K}-1}$  are physically interpreted as “nearest-neighbor hopping amplitudes” on this one-dimensional *Krylov chain* with  $\phi_n(t)$  being the “wavefunction” of the moving “particle” along the chain. The definition of Krylov complexity then is given by  $K(t) \equiv \sum_{n=0}^{\mathcal{K}-1} n |\phi_n(t)|^2$ .

The UOGH [13] implies  $b_n \sim n$  for chaotic systems. Then, as shown in [23], there is a saturation of  $b_n \rightarrow 1$ , emblematic of random matrix theory [23]. Recall that the eigenvalues of chaotic systems are extensive in its degrees of freedom while the eigenvalues for a random matrix Hamiltonian is usually scaled to be of  $\mathcal{O}(1)$ . That’s why in order to compare the growth of operators with the random matrix behavior, we need to properly scale our results which is explained in the supplemental material.

*Main Results.*— The following picture emerges from the aforementioned discussions for chaotic systems with  $f$ -degrees of freedom between the dual behavior of Lanczos coefficients  $\{b_n\}$  and Krylov complexity  $K(t)$  [17, 61]: (1) initially a linear growth of  $\{b_n\}$  for  $1 \ll n < \mathcal{O}(f)$  implies an exponential growth in time of  $K(t)$  for  $0 \lesssim t < \mathcal{O}(\log(f))$  as captured by the UOGH [13], (2) a saturation after the linear growth happens for  $\{b_n\}$  for  $n \gg \mathcal{O}(f)$  that implies a linear-in-time growth of  $K(t)$

for  $t \gtrsim \mathcal{O}(\log(f))$ , and (3) finally the descent of  $\{b_n\}$  to zero for  $n \sim \mathcal{O}(e^{2f})$  implying a saturation of  $K(t)$  for  $t \sim \mathcal{O}(e^{2f})$ . The last stage happens at extremely late time scale that is beyond the scope of this work.

We only consider local operators having zero overlap with other conserved quantities of the system. Stage (1) of the complexity growth still has notion of locality from the point of view of operators. For ergodic systems, a random matrix behavior sets in during stage (2) of the evolution, allowing for a universal description of operators because the notion of locality is lost. Therefore, our analysis starts *after* stage (1) of complexity growth.

Since the Krylov chain is a tight-binding model with disorder in the hopping elements, it is natural to expect phenomenology of Anderson localization (see, e.g., [18, 62] for an integrable system). For a fixed length of the Krylov chain, we propose the inverse of localization length given by the square root of

$$\sigma^2 = \text{Var}(x_j) \quad \text{where} \quad x_j \equiv \ln\left(\frac{b_{2j-1}}{b_{2j}}\right), \quad (1)$$

as a probe to quantitatively detect weak ergodicity-breaking transition points. We will refer to this as the *Krylov variance* or simply *variance* for brevity from this point on. We note the differences from the two related works [18, 26]. The variance was studied in the context of integrable and weak-integrability broken systems in [18] where they studied the localization on the Krylov chain in a qualitative sense. Furthermore, the variance was used in [26] to find correlations with quantum chaos where they included the entire spectrum of Lanczos coefficients including the stage 1 of the aforementioned complexity growth where the notion of operator locality is still present. We fundamentally differ from their analyses in the following ways: (a) we propose the Krylov variance as a probe for ergodicity/weak ergodicity-breaking transition, (b) we only include the Lanczos coefficients after the scrambling time (stage 2) where a sensible universal description of operators becomes viable, and (c) we provide a quantitative tool to predict the point of transition through a collapse for an arbitrary local operator across different system sizes after the scrambling time.

We wish to clarify that the Krylov variance can still be employed when keeping the entire sequence of  $\{b_n\}$  (as we show for the case of the large- $q$  SYK model below, also see supplementary material) but the collapse and the universality across different operators can only be understood in qualitative terms. The quantitative analysis of transition points observed through collapse can only be captured after the scrambling time. Conceptually, the localization length is enhanced for integrable systems as shown in [18] and we show via the analytical case of the large- $q$  SYK model that for the ergodic regime,  $\sigma^2 \rightarrow 0$  for  $n \rightarrow \infty$ . Therefore the ergodicity/weak ergodicity-breaking transition is mapped to a complete delocalization/localization phenomenology on the Krylov chain.

An alternative analysis to probe quantum thermalization has been done in [63, 64] where they use the Lanczos

algorithm for eigenstates (unlike the operator Lanczos algorithm we use in this work) which generates a completely different Krylov basis than ours, therefore fundamentally differing from our approach.

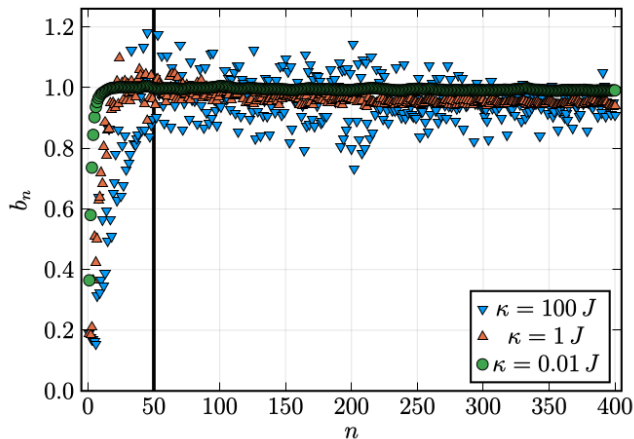


Figure 1: Lanczos coefficients  $\{b_n\}$  at  $\beta = 0$  in a single realization of the Majorana SYK model (Eq. (2)) where  $N = 26$ , the initial operator is  $|\mathcal{O}_0\rangle = \chi_1$ . The vertical solid line at  $n = 50$  indicates where the initial ramp of the  $b_n$  has seized for all parameter values.

*SYK Model.*— Quantum ergodicity of the Majorana SYK model has been studied in [65, 66] where in the limit of large numbers of particles, the system is ergodic. Here we start by considering a general case of the large- $q$  SYK model whose Hamiltonian is given by  $\mathcal{H}_q = i^{q/2} \sum_{1 \leq i_1 < \dots < i_q \leq N} J_{i_1 \dots i_q} \chi_{i_1} \dots \chi_{i_q}$  (subscript  $q$  denotes  $q$ -body interaction). Here  $\chi_i$  are the Majorana fermions and  $J_{i_1 \dots i_q}$  are random variables derived from a Gaussian ensemble with zero mean and variance  $\frac{(q-1)! \mathcal{J}^2}{2qN^{q-1}}$  where we have introduced a re-scaled interaction strength  $\mathcal{J} \equiv 2^{1-q} q J$  for some constant  $J$ . The dimension of the Hilbert space is  $\mathcal{N} = 2^{N/2}$ . We consider the large- $N$  semi-classical limit where the system is ergodic as studied in [65]. Using the large- $q$  expansion [48], we can calculate the auto-correlation function corresponding to an initial operator, say  $|\mathcal{O}_o\rangle = \chi_1(t=0)$  that in turn leads to analytical evaluation of (non-rescaled) Lanczos coefficients  $\{b_n\}$  for all  $n$  [13]. In the infinite temperature limit at  $\mathcal{O}(q^0)$ , we get  $b_n = \mathcal{J} \sqrt{n(n-1)} + \mathcal{O}(1/q)$  for  $n > 1$  [67]. Therefore we can calculate the variance as in Eq. (1) and find by including the entire sequence of  $\{b_n\}$  that  $\sigma^2 \rightarrow 0$  as  $n \rightarrow \infty$ . Therefore, on the level of the Krylov chain, we find a delocalization in contrast to the localization that happens in the weakly ergodicity-broken regime where  $\sigma^2$  is enhanced. Using this as a motivation, we study a system of coupled SYK models

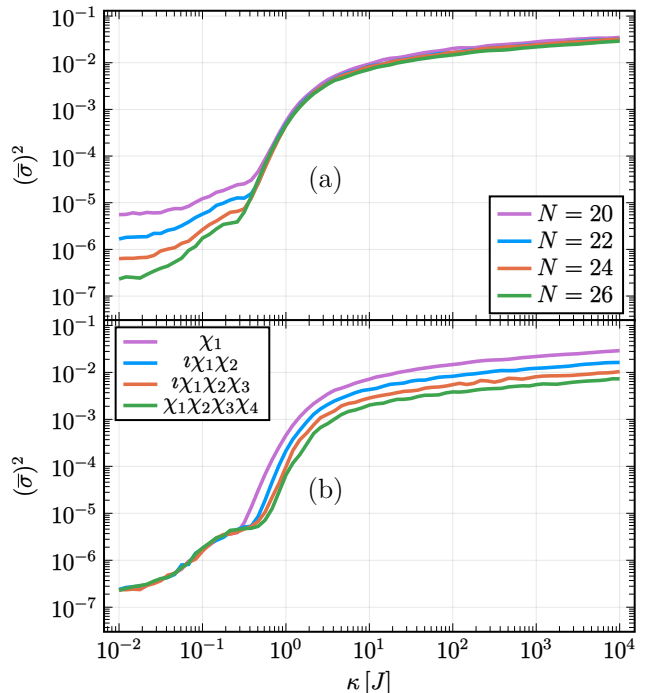


Figure 2: Krylov variance  $\sigma^2$  at  $\beta = 0$  against the system parameter  $\kappa$  for the coupled SYK model (Eq. (2)) ignoring the first 50 Lanczos coefficients  $\{b_n\}$  as justified through Fig. 1 in the text. We have calculated the average  $\bar{\sigma}$  from a total of 5 realizations before calculating  $(\bar{\sigma})^2$ . In (a), we use  $|\mathcal{O}_0\rangle = \chi_1$  where the collapse of different system sizes captures the point of weak ergodicity-breaking. In (b), we show universal behavior across different operators for  $N = 26$  where there is a qualitative change in behavior around the transition point.

whose Hamiltonian is given by

$$\mathcal{H} = \frac{2}{\sqrt{N}} \sum_{1 \leq i < j < k < l \leq N} J_{ijkl} \chi_i \chi_j \chi_k \chi_l + \nu \sum_{1 \leq i < j \leq N} \kappa_{ij} \chi_i \chi_j. \quad (2)$$

The random couplings  $J_{ijkl}$  and  $\kappa_{ij}$  are drawn from a Gaussian distribution with variance  $\frac{6J^2}{N^3}$  and  $\frac{\kappa^2}{N}$  respectively, where  $J$  and  $\kappa$  are system parameters. We measure  $\kappa$  in units of  $J$  and we fix the unit system on the energy scale  $J = 1$ . By tuning  $\kappa$ , we can study the ergodic and weakly ergodicity-broken regimes. This model has also been considered in [38] where they study thermalization dynamics of this model. They employ the adiabatic gauge potential (AGP) and analyze the Thouless time via the spectral form factor [37]. In their analysis using AGP, they find a weak ergodicity-breaking transition defined in terms of deviation from the ETH scaling. Finding this deviation from the ETH prediction leads to a delayed thermalization as can be seen from the spectral form factor. Here we study the same weak ergodicity-breaking transition.

We observe a linear ramp in the sequence of  $\{b_n\}$  in Fig. 1 for the ergodic regime ( $\kappa = 0.01J$ ) as expected from UOGH [13]. The vertical solid line at  $n = 50$  shows the end of this initial ramp and the onset of random matrix behavior beyond which we argue that all operators attain universal behavior due to the lost notion of locality. We note the large spread in the sequence of  $\{b_n\}$  in the ergodicity-broken regime ( $\kappa = 100J$ ) which we quantify by studying the Krylov variance  $\sigma^2$  (Eq. (1)) beyond the scrambling point ( $n \geq 50$ ). We plot the Krylov variance in Fig. 2 against  $\kappa$ . In Fig. 2(a), we find a near perfect collapse across different system sizes for the initial operator  $|\mathcal{O}_0\rangle = \chi_1$ , capturing the weak ergodicity-breaking transition. This transition is also captured in [38] (first proposed in [68]) where they observe a deviation from the ETH scaling of the AGP that leads to delayed thermalization as analyzed via the spectral form factor. As can be seen in Fig. 2(a) the value of  $\sigma^2$  diminishes in the ergodic regime with increasing system size, while it is enhanced in the weakly ergodicity-broken regime. This signals delocalization and localization on the Krylov chain, respectively. In order to show universal behavior across different operators, we plot the Krylov variance for different operators at  $N = 26$  in Fig. 2(b). We do observe a qualitatively universal change of behavior across the transition point. Again, we observe a near perfect collapse in the ergodic regime signalling *universality*. In the supplemental material, we also provide plots for a single realization of the coupled SYK model which is not far from multiple realizations as shown here and for the full sequence of  $\{b_n\}$ .

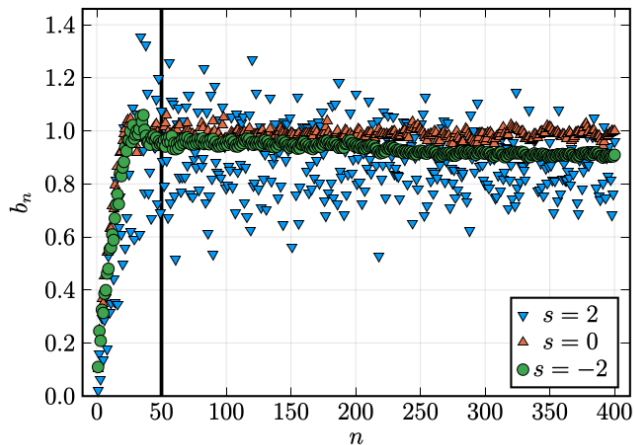


Figure 3: Lanczos coefficients  $\{b_n\}$  at  $\beta = 0$  in the quantum East model (Eq. (3)) for  $L = 13$  where the initial operator is  $|\mathcal{O}_0\rangle = n_6$ . The vertical solid line ( $n = 50$ ) shows the value of  $n$  where the initial ramp of the Lanczos coefficients ends for all considered parameter values.

*Quantum East Model.*— The Hamiltonian of the quan-

tum East model is defined on a 1D lattice of size  $L$

$$\mathcal{H} = -\frac{1}{2} \sum_{i=1}^{L-1} n_i (e^{-s} \sigma_{i+1}^x - \mathbb{1}), \quad (3)$$

where  $n_i$  is the projection on the spin-up state at lattice site  $i$ ,  $\sigma_i^x$  is the  $x$ -Pauli operator acting on that respective lattice site  $i$  and  $s$  is a system parameter. As  $n_i$  projects on the spin-up state we can effectively consider any spin-down lattice site as a kinetic constraint for dynamics on the next lattice site.

For appropriate boundary conditions, the ground-state of the quantum East model undergoes a sharp delocalization ( $s < 0$ )/localization ( $s > 0$ ) transition at  $s = 0$  [52] (see the supplemental material for further details). Moreover in the regime  $s \geq 0$ , localized eigenstates can be constructed at arbitrary energy density. We analyze this model and find that there exists a weak ergodicity-breaking around  $s = 0$ .

Similar to the SYK case, we first plot the Lanczos coefficients  $\{b_n\}$  in Fig. 3, where we observe a qualitatively different spreading in the sequence of  $\{b_n\}$  between the ergodic and non-ergodic regime. In particular, we again observe a linear ramp in the ergodic regime  $s = -2$  as expected from the UOGH [13] followed by a saturation as denoted by the vertical solid line, reminiscent of random matrix type behavior. To quantify the spread of  $\{b_n\}$ , we plot the Krylov variance  $\sigma^2$  against  $s$  in Fig. 4, ignoring the  $\{b_n\}$  of the initial ramp. Around the transition point  $s = 0$  we observe a qualitative change across different system sizes in Fig. 4(a), signifying weak ergodicity-breaking with a subsequent collapse of the curves around  $s > 1$ . The quantum East model is already known to have a first order phase transition at  $s = 0$  [69, 70]. At the transition point  $s = 0$ , some eigenstates of the system undergo a sharp delocalization/localization transition which leads to non-thermal behavior and delayed relaxation to thermalization [52]. This delayed thermalization is manifested as weak ergodicity-breaking as already discussed in the introduction and this is indeed the point also captured by the Krylov variance in Fig. 4(a). We leave the discussion of the collapse around  $s = 1$  for future work. Fig. 4(b) captures how operators in the bulk of the system show universal behavior in the ergodic regime and across the transition, similar to the behavior in the coupled SYK model (Fig. 2(b)).

*Conclusions and Discussion.*— The UOGH [13] mapped the question of quantum chaos and operator complexity to a semi-infinite tight-binding Krylov chain. Here we argued that a universal scaling for all local operators is viable only after the scrambling time where the behavior is reminiscent of a random matrix theory. We propose the measure of the inverse localization length (Eq. (1)) on the Krylov chain as a probe for capturing weak ergodicity-breaking by showing the collapse across different system sizes. We also showed a universal behavior for different local operators across the transition point. Conceptually, we argued and then showed that

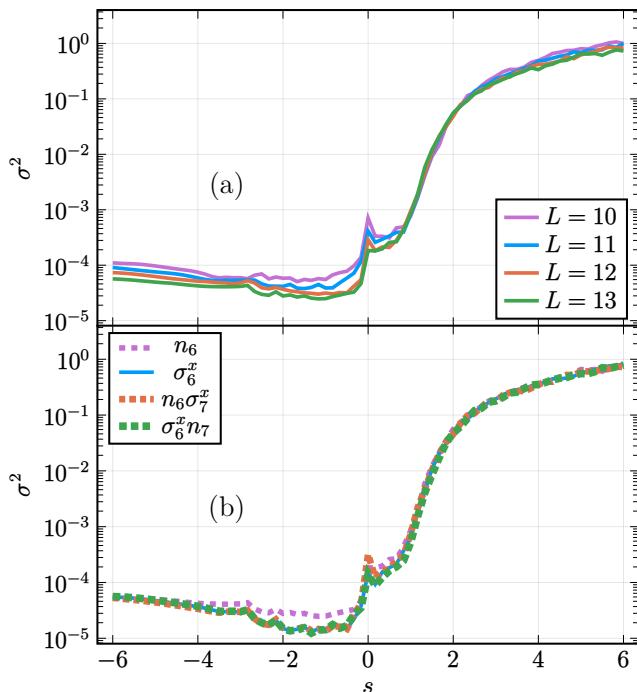


Figure 4: Krylov variance  $\sigma^2$  at  $\beta = 0$  against the system parameter  $s$  in the quantum East model (Eq. (3)) for different system sizes. We ignore the first 50 Lanczos coefficients  $\{b_n\}$  as justified through Fig. 3 in the text. In (a), we use  $|\mathcal{O}_0\rangle = n_{\lfloor L/2 \rfloor}$  as an operator with support on the middle of the lattice. A qualitative change in  $\sigma^2$  around  $s = 0$  and subsequent collapse across different system sizes capture the transition point that leads to weak ergodicity-breaking. We note that the peak at  $s = 0$  decreases with the system size. In (b), we plot for  $L = 13$  where the purpose is to show the qualitatively universal behavior of different operators across the transition point.

considerations after the scrambling time allows for the Krylov variance in Eq. (1) to be used as a quantitative tool to find the transition point. Therefore we boiled down the question of ergodicity/weak ergodicity-breaking to delocalization/localization phenomenology on the Krylov chain. The next logical extension is to generalize the findings to finite temperatures, where one has to use the Wightman inner-product as discussed above. The natural question to ask is about the universality of the Krylov variance can be answered by matching against other approaches for studying ergodicity breaking, in particular the adiabatic gauge potential (AGP) [12, 37] following the analytical efforts made in [71]. This means further inquiring into the nature of integrable systems and associated weak-integrability breaking. In this work we already compared the results for the coupled SYK model where we captured the same point of weak ergodicity-breaking where the ETH scaling is violated for the AGP leading to delayed thermalization [38]. We believe that the “raw” Lanczos coefficients shown in Figs. 1 and 3 capture a variety of physics, e.g., ergodicity breaking, phase transitions, etc. Different constructions of the Lanczos coefficients, such as the Krylov variance proposed in this work, *may* capture different aspects of the underlying physics. Another playground for exploration can be open quantum systems as studied in [27–30].

*Acknowledgments.*— We are grateful to Salvatore R. Manmana, Fabian Heidrich-Meisner, Stefan Kehrein and Miroslav Hopjan for helpful insights and discussion. This work was supported by Deutsche Forschungsgemeinschaft (DFG, German Research Foundation) – 217133147, 499180199, 436382789, 493420525; via CRC 1073 (project B03), FOR 5522, and large equipment grants (GOEGrid).

- 
- [1] L. D. Landau and E. M. Lifshitz, *Course of Theoretical Physics, Vol. 9 Statistical Physics, Part-2* (Elsevier India, 2014).
- [2] B. M. Victor and M. Tabor, Level clustering in the regular spectrum, *Proc. R. Soc. Lond. A* **356**, 375 (1977).
- [3] M. V. Berry, Regular and irregular semiclassical wavefunctions, *J. Phys. A: Math. Gen.* **10**, 2083 (1977).
- [4] J. M. Deutsch, Quantum statistical mechanics in a closed system, *Phys. Rev. A* **43**, 2046 (1991).
- [5] M. Srednicki, Chaos and quantum thermalization, *Phys. Rev. E* **50**, 888 (1994).
- [6] M. Srednicki, Thermal fluctuations in quantized chaotic systems, *J. Phys. A: Math. Gen.* **29**, L75 (1996).
- [7] M. Srednicki, The approach to thermal equilibrium in quantized chaotic systems, *J. Phys. A: Math. Gen.* **32**, 1163 (1999).
- [8] M. Rigol, V. Dunjko, and M. Olshanii, Thermalization and its mechanism for generic isolated quantum systems, *Nature* **452**, 854 (2008).
- [9] L. D’Alessio, Y. Kafri, A. Polkovnikov, and M. Rigol, From quantum chaos and eigenstate thermalization to statistical mechanics and thermodynamics, *Adv. Phys.* (2016).
- [10] J. M. Deutsch, Eigenstate thermalization hypothesis, *Rep. Prog. Phys.* **81**, 082001 (2018).
- [11] D. A. Abanin, E. Altman, I. Bloch, and M. Serbyn, Colloquium: Many-body localization, thermalization, and entanglement, *Rev. Mod. Phys.* **91**, 021001 (2019).
- [12] C. Lim, K. Matirko, A. Polkovnikov, and M. O. Flynn, Defining classical and quantum chaos through adiabatic transformations, arXiv 10.48550/arXiv.2401.01927 (2024), 2401.01927.
- [13] D. E. Parker, X. Cao, A. Avdoshkin, T. Scaffidi, and E. Altman, A Universal Operator Growth Hypothesis, *Phys. Rev. X* **9**, 041017 (2019).
- [14] E. Rabinovici, A. Sánchez-Garrido, R. Shir, and J. Son-

- ner, Operator complexity: a journey to the edge of Krylov space, *J. High Energy Phys.* **2021** (6), 1.
- [15] P. Caputa, J. M. Magan, and D. Patramanis, Geometry of Krylov complexity, *Phys. Rev. Res.* **4**, 013041 (2022).
- [16] F. Ballar Trigueros and C.-J. Lin, Krylov complexity of many-body localization: Operator localization in Krylov basis, *SciPost Phys.* **13**, 037 (2022).
- [17] E. Rabinovici, A. Sánchez-Garrido, R. Shir, and J. Sonner, Krylov complexity from integrability to chaos, *J. High Energy Phys.* **2022** (7), 1.
- [18] E. Rabinovici, A. Sánchez-Garrido, R. Shir, and J. Sonner, Krylov localization and suppression of complexity, *J. High Energy Phys.* **2022** (3), 1.
- [19] B. Bhattacharjee, X. Cao, P. Nandy, and T. Pathak, Krylov complexity in saddle-dominated scrambling, *J. High Energy Phys.* **2022** (5), 1.
- [20] B. Bhattacharjee, P. Nandy, and T. Pathak, Krylov complexity in large  $q$  and double-scaled SYK model, *J. High Energy Phys.* **2023** (8), 1.
- [21] A. Bhattacharya, P. P. Nath, and H. Sahu, Krylov complexity for non-local spin chains, arXiv [10.48550/arXiv.2312.11677](https://arxiv.org/abs/10.48550/arXiv.2312.11677) (2023), [2312.11677](https://arxiv.org/abs/2312.11677).
- [22] A. Bhattacharyya, D. Ghosh, and P. Nandi, Operator growth and Krylov complexity in Bose-Hubbard model, *J. High Energy Phys.* **2023** (12), 1.
- [23] H. Tang, Operator Krylov complexity in random matrix theory, arXiv [10.48550/arXiv.2312.17416](https://arxiv.org/abs/10.48550/arXiv.2312.17416) (2023), [2312.17416](https://arxiv.org/abs/2312.17416).
- [24] H. A. Camargo, V. Jahnke, H.-S. Jeong, K.-Y. Kim, and M. Nishida, Spectral and Krylov complexity in billiard systems, *Phys. Rev. D* **109**, 046017 (2024).
- [25] P. Caputa, H.-S. Jeong, S. Liu, J. F. Pedraza, and L.-C. Qu, Krylov complexity of density matrix operators, arXiv [10.48550/arXiv.2402.09522](https://arxiv.org/abs/10.48550/arXiv.2402.09522) (2024), [2402.09522](https://arxiv.org/abs/2402.09522).
- [26] K. Hashimoto, K. Murata, N. Tanahashi, and R. Watanabe, Krylov complexity and chaos in quantum mechanics, *J. High Energy Phys.* **2023** (11), 1.
- [27] A. Bhattacharya, P. Nandy, P. P. Nath, and H. Sahu, Operator growth and Krylov construction in dissipative open quantum systems, *J. High Energy Phys.* **2022** (12), 1.
- [28] B. Bhattacharjee, X. Cao, P. Nandy, and T. Pathak, Operator growth in open quantum systems: lessons from the dissipative SYK, *J. High Energy Phys.* **2023** (3), 1.
- [29] A. Bhattacharya, P. Nandy, P. P. Nath, and H. Sahu, On Krylov complexity in open systems: an approach via bi-Lanczos algorithm, *J. High Energy Phys.* **2023** (12), 1.
- [30] C. Liu, H. Tang, and H. Zhai, Krylov complexity in open quantum systems, *Phys. Rev. Res.* **5**, 033085 (2023).
- [31] A. Dymarsky and M. Smolkin, Krylov complexity in conformal field theory, *Phys. Rev. D* **104**, L081702 (2021).
- [32] R. Heveling, J. Wang, and J. Gemmer, Numerically probing the universal operator growth hypothesis, *Phys. Rev. E* **106**, 014152 (2022).
- [33] A. Avdoshkin, A. Dymarsky, and M. Smolkin, Krylov complexity in quantum field theory, and beyond, arXiv [10.48550/arXiv.2212.14429](https://arxiv.org/abs/10.48550/arXiv.2212.14429) (2022), [2212.14429](https://arxiv.org/abs/2212.14429).
- [34] K. Adhikari, S. Choudhury, and A. Roy, Krylov Complexity in Quantum Field Theory, *Nucl. Phys. B* **993**, 116263 (2023).
- [35] T. Xu, T. Scaffidi, and X. Cao, Does Scrambling Equal Chaos?, *Phys. Rev. Lett.* **124**, 140602 (2020).
- [36] N. Dowling, P. Kos, and K. Modi, Scrambling Is Necessary but Not Sufficient for Chaos, *Phys. Rev. Lett.* **131**, 180403 (2023).
- [37] M. Pandey, P. W. Claeys, D. K. Campbell, A. Polkovnikov, and D. Sels, Adiabatic Eigenstate Deformations as a Sensitive Probe for Quantum Chaos, *Phys. Rev. X* **10**, 041017 (2020).
- [38] D. K. Nandy, T. Čadež, B. Dietz, A. Andreanov, and D. Rosa, Delayed thermalization in the mass-deformed Sachdev-Ye-Kitaev model, *Phys. Rev. B* **106**, 245147 (2022).
- [39] P. Sala, T. Rakovszky, R. Verresen, M. Knap, and F. Pollmann, Ergodicity Breaking Arising from Hilbert Space Fragmentation in Dipole-Conserving Hamiltonians, *Phys. Rev. X* **10**, 011047 (2020).
- [40] V. Khemani, M. Hermele, and R. Nandkishore, Localization from Hilbert space shattering: From theory to physical realizations, *Phys. Rev. B* **101**, 174204 (2020).
- [41] C. J. Turner, A. A. Michailidis, D. A. Abanin, M. Serbyn, and Z. Papić, Weak ergodicity breaking from quantum many-body scars, *Nat. Phys.* **14**, 745 (2018).
- [42] M. Serbyn, D. A. Abanin, and Z. Papić, Quantum many-body scars and weak breaking of ergodicity, *Nat. Phys.* **17**, 675 (2021).
- [43] G.-X. Su, H. Sun, A. Hudomal, J.-Y. Desaulles, Z.-Y. Zhou, B. Yang, J. C. Halimeh, Z.-S. Yuan, Z. Papić, and J.-W. Pan, Observation of many-body scarring in a Bose-Hubbard quantum simulator, *Phys. Rev. Res.* **5**, 023010 (2023).
- [44] J.-Y. Desaulles, A. Hudomal, D. Banerjee, A. Sen, Z. Papić, and J. C. Halimeh, Prominent quantum many-body scars in a truncated Schwinger model, *Phys. Rev. B* **107**, 205112 (2023).
- [45] J. C. Halimeh, L. Barbiero, P. Hauke, F. Grusdt, and A. Bohrdt, Robust quantum many-body scars in lattice gauge theories, *Quantum* **7**, 1004 (2023), [2203.08828v5](https://arxiv.org/abs/2203.08828v5).
- [46] S. Sachdev and J. Ye, Gapless spin-fluid ground state in a random quantum Heisenberg magnet, *Phys. Rev. Lett.* **70**, 3339 (1993).
- [47] A. Kitaev, A simple model of quantum holography (2015), Talks given at “KITP: Entanglement in Strongly-Correlated Quantum Matter”, (Part 1, Part 2).
- [48] J. Maldacena and D. Stanford, Remarks on the Sachdev-Ye-Kitaev model, *Phys. Rev. D* **94**, 106002 (2016).
- [49] D. Chowdhury, A. Georges, O. Parcollet, and S. Sachdev, Sachdev-Ye-Kitaev models and beyond: Window into non-Fermi liquids, *Rev. Mod. Phys.* **94**, 035004 (2022).
- [50] M. van Horssen, E. Levi, and J. P. Garrahan, Dynamics of many-body localization in a translation-invariant quantum glass model, *Phys. Rev. B* **92**, 100305 (2015).
- [51] P. Crowley, *Entanglement and Thermalization in Many Body Quantum Systems*, Ph.D. thesis, University College London (2023), <https://discovery.ucl.ac.uk/id/eprint/1553310>.
- [52] N. Pancotti, G. Giudice, J. I. Cirac, J. P. Garrahan, and M. C. Bañuls, Quantum East Model: Localization, Non-thermal Eigenstates, and Slow Dynamics, *Phys. Rev. X* **10**, 021051 (2020).
- [53] B. Bertini, P. Kos, and T. Prosen, Localized dynamics in the floquet quantum east model, *Phys. Rev. Lett.* **132**, 10.1103/physrevlett.132.080401 (2024).
- [54] R. Nandkishore and D. A. Huse, Many-Body Localization and Thermalization in Quantum Statistical Mechanics, *Annu. Rev. Condens. Matter Phys.* **6**, 15 (2015).
- [55] K. Royen, S. Mondal, F. Pollmann, and F. Heidrich-

- Meisner, Enhanced many-body localization in a kinetically constrained model, *Phys. Rev. E* **109**, 10.1103/physreve.109.024136 (2024).
- [56] A. Chandran, T. Iadecola, V. Khemani, and R. Moessner, Quantum many-body scars: A quasiparticle perspective, *Annual Review of Condensed Matter Physics* **14**, 443 (2023).
- [57] P. Brighi, M. Ljubotina, and M. Serbyn, Hilbert space fragmentation and slow dynamics in particle-conserving quantum east models, *SciPost Physics* **15**, 10.21468/scipostphys.15.3.093 (2023).
- [58] In the literature on Krylov complexity, another physically equivalent definition of Liouvillian has also been used, namely  $\tilde{\mathcal{L}} \equiv [\mathcal{H}, \bullet]$ . We have proved the equivalence of both the definitions and the consequent analyses in the supplemental material.
- [59] V. S. Viswanath and G. Müller, *The Recursion Method* (Springer, Berlin, Germany, 1994).
- [60] As derived in the supplemental material, if we would use a different expansion coefficient for the operator such as  $|\mathcal{O}(t)\rangle = \sum_{n=0}^{K-1} v^n \psi_n(t) |\mathcal{O}_n\rangle$ , then we obtain a “Schroödinger-type” structure, namely  $i\partial_t \psi_n(t) = b_n \psi_{n-1}(t) - b_{n+1} \psi_{n+1}(t)$ . The coefficients  $\phi_n(t)$  and  $\psi_n(t)$  are related through  $\phi_n(t) = v^n \psi_n(t)$ .
- [61] J. L. F. Barbón, E. Rabinovici, R. Shir, and R. Sinha, On the evolution of operator complexity beyond scrambling, *J. High Energy Phys.* **2019** (10), 1.
- [62] L. Fleishman and D. C. Licciardello, Fluctuations and localization in one dimension, *J. Phys. C: Solid State Phys.* **10**, L125 (1977).
- [63] B. Bhattacharjee, S. Sur, and P. Nandy, Probing quantum scars and weak ergodicity breaking through quantum complexity, *Phys. Rev. B* **106**, 205150 (2022).
- [64] M. Alishahiha and M. J. Vasli, Thermalization in Krylov Basis, *arXiv* (2024), 2403.06655.
- [65] A. M. Garcia-Garcia and J. J. M. Verbaarschot, Spectral and thermodynamic properties of the Sachdev-Ye-Kitaev model, *Phys. Rev. D* **94**, 126010 (2016).
- [66] A. Altland and D. Bagrets, Quantum ergodicity in the SYK model, *Nucl. Phys. B* **930**, 45 (2018).
- [67]  $b_1$  is of the order  $\mathcal{O}(\frac{1}{\sqrt{q}})$ .
- [68] F. Monteiro, T. Micklitz, M. Tezuka, and A. Altland, Minimal model of many-body localization, *Phys. Rev. Res.* **3**, 013023 (2021).
- [69] J. P. Garrahan, R. L. Jack, V. Lecomte, E. Pitard, K. van Duijvendijk, and F. van Wijland, Dynamical First-Order Phase Transition in Kinetically Constrained Models of Glasses, *Phys. Rev. Lett.* **98**, 195702 (2007).
- [70] M. C. Bañuls and J. P. Garrahan, Using matrix product states to study the dynamical large deviations of kinetically constrained models, *Phys. Rev. Lett.* **123**, 200601 (2019).
- [71] B. Bhattacharjee, A Lanczos approach to the Adiabatic Gauge Potential, *arXiv* 10.48550/arXiv.2302.07228 (2023), 2302.07228.

# Supplemental Material — Krylov localization as a probe for ergodicity breaking

Heiko Georg Menzler<sup>1,\*</sup> and Rishabh Jha<sup>1,†</sup>

<sup>1</sup>*Institute for Theoretical Physics, Georg-August-Universität Göttingen,  
Friedrich-Hund-Platz 1, 37077 Göttingen, Germany*

## CONTENTS

I. Review of Lanczos approach to Krylov complexity	1
A. Krylov space of operators	1
B. Lanczos algorithm and the Krylov basis	2
C. Stability of the Lanczos algorithm	3
D. Krylov complexity	4
E. Growth of Krylov complexity	5
1. Universal Operator Growth Hypothesis	5
2. Random matrix theory	5
3. Decay at the edge of Krylov space	5
4. Summary	5
F. Krylov chain	6
G. Equivalence of different approaches	6
II. Coupled Sachdev-Ye-Kitaev model	7
III. Quantum East model	11
References	12

## I. REVIEW OF LANCZOS APPROACH TO KRYLOV COMPLEXITY

### A. Krylov space of operators

We consider a vector space of bounded operators in the Hilbert space  $\mathbf{H}$  denoted by  $\mathcal{B}(\mathbf{H})$ . If we consider the dimension of the Hilbert space  $\mathbf{H}$  as  $\mathcal{N}$ , then the dimension of the vector space of bounded operators  $\mathcal{B}(\mathbf{H})$  is  $\mathcal{N}^2$ . Now if we consider any initial operator  $\mathcal{O}_0 \in \mathcal{B}(\mathbf{H})$  where  $\mathcal{O}_0 = \mathcal{O}(t=0)$ , then the time evolution of the operator in Heisenberg picture for a given time-independent Hamiltonian  $\mathcal{H}$  is given by

$$\mathcal{O}(t) = e^{i\mathcal{H}t} \mathcal{O}_0 e^{-i\mathcal{H}t} \quad (1)$$

Using the Baker-Campbell-Hausdorff formula, we get

$$\begin{aligned} \mathcal{O}(t) &= \mathcal{O}_0 + it[\mathcal{H}, \mathcal{O}_0] + \frac{(it)^2}{2!} [\mathcal{H}, [\mathcal{H}, \mathcal{O}_0]] + \frac{(it)^3}{3!} [\mathcal{H}, [\mathcal{H}, [\mathcal{H}, \mathcal{O}_0]]] + \dots \\ &= \sum_{n=0}^{\infty} \frac{t^n}{n!} \mathcal{L}^n \mathcal{O}_0 \end{aligned} \quad (2)$$

where Liouvillian operator  $\mathcal{L} \equiv i[H, \bullet]$  acts as, for instance,  $\mathcal{L}\mathcal{O}_0 = i[\mathcal{H}, \mathcal{O}_0]$  and  $\mathcal{L}^2\mathcal{O}_0 = i^2[\mathcal{H}, [\mathcal{H}, \mathcal{O}_0]]$ . Since Krylov complexity is defined in terms of evolution of operator in  $\mathcal{B}(\mathbf{H})$  for a given Hamiltonian  $\mathcal{H}$ , it's easier to study the vector space by using the operator-to-state mapping  $\mathcal{O} \rightarrow |\mathcal{O}\rangle$ . In this notation, we have

$$|\mathcal{O}(t)\rangle = e^{\mathcal{L}t} |\mathcal{O}_0\rangle = \sum_{n=0}^{\infty} \frac{t^n}{n!} |\mathcal{L}^n \mathcal{O}_0\rangle \quad (3)$$

\* [heiko.menzler@uni-goettingen.de](mailto:heiko.menzler@uni-goettingen.de)

† [rishabh.jha@uni-goettingen.de](mailto:rishabh.jha@uni-goettingen.de)



Each  $|\mathcal{L}^n \mathcal{O}_0\rangle$  for a particular value of  $n$  is independent from others and this forms the basis for Krylov space that is spanned by

$$\text{Krylov space} = \text{span} [|\mathcal{O}_0\rangle, |\mathcal{L}^1 \mathcal{O}_0\rangle, |\mathcal{L}^2 \mathcal{O}_0\rangle, \dots] \quad (4)$$

We employ the Lanczos algorithm where we first need to define the inner-product on  $\mathcal{B}(\mathbf{H})$ . We chose the Wightman inner-product

$$(A|B) = \langle e^{-\beta\mathcal{H}/2} A^\dagger e^{-\beta\mathcal{H}/2} B \rangle_\beta \quad (5)$$

where  $\langle \dots \rangle_\beta = \text{Tr}[e^{-\beta\mathcal{H}} \dots] / \text{Tr}[e^{-\beta\mathcal{H}}]$ . Since we are interested in the infinite temperature limit (inverse temperature  $\beta = 0$ ), the inner produce reduces to

$$(A|B) = \frac{1}{\mathcal{N}} \text{Tr}[A^\dagger B] \quad (6)$$

where  $\mathcal{N}$  is the dimension of the Hilbert space  $\mathbf{H}$ .

### B. Lanczos algorithm and the Krylov basis

We present the operator Lanczos algorithm for infinite temperature case ( $\beta = 0$ ) where inner produce becomes Eq. (6) but generalizing to finite temperature case is straightforward using Eq. (5).

We start with an initial operator that is properly normalized, namely  $|\mathcal{O}_0\rangle \rightarrow \frac{1}{\sqrt{(\mathcal{O}_0|\mathcal{O}_0)}} |\mathcal{O}_0\rangle$ . Then the procedure is

1. Set  $b_0 \equiv 0$  and  $\mathcal{O}_{-1} = 0$ .
2. For  $n \geq 1$  :  $|A_n\rangle = |\mathcal{L}\mathcal{O}_{n-1}\rangle - b_{n-1}|\mathcal{O}_{n-2}\rangle$ .
3. Set  $b_n = \sqrt{(A_n|A_n)}$ .
4. Stop if  $b_n = 0$ , else set  $|\mathcal{O}_n\rangle = \frac{|A_n\rangle}{b_n}$  and jump to step 2.

This procedure will construct a set of basis vectors that are normalized and orthogonal to each other

$$\text{Krylov basis} = \{|\mathcal{O}_n\rangle\}_{n=0}^{\mathcal{K}-1} \quad (7)$$

as well as a set of Lanczos coefficients  $\{b_n\}_{n=1}^{\mathcal{K}-1}$ . Here  $\mathcal{K}$  is the Krylov space dimension which is bounded from above as follows [1]:

$$\mathcal{K} \leq \mathcal{N}^2 - \mathcal{N} + 1 \quad (8)$$

We always initiate our algorithm with a Hermitian operator  $|\mathcal{O}_0\rangle$ . The Lanczos coefficients allow us to represent the Liouvillian operator  $\mathcal{L}$  as a tri-diagonal matrix where the off-diagonal elements are the Lanczos coefficients  $\{b_n\}$  while the diagonal elements are identically zero due to the structure of the Liouvillian operator that implies  $(\mathcal{O}_n|\mathcal{L}|\mathcal{O}_n) = 0 \forall n$ . To explicitly construct the matrix, let's evaluate the arbitrary matrix element  $(\mathcal{O}_m|\mathcal{L}|\mathcal{O}_n)$  as follows:

$$(\mathcal{O}_m|\mathcal{L}|\mathcal{O}_n) = (\mathcal{O}_m|[A_{n+1}] + b_n|\mathcal{O}_{n-1}\rangle) = b_{n+1} \underbrace{(\mathcal{O}_m|\mathcal{O}_{n+1}\rangle)}_{=\delta_{m,n+1}} + b_n \underbrace{(\mathcal{O}_m|\mathcal{O}_{n-1}\rangle)}_{=\delta_{m,n-1}} = \begin{cases} b_{n+1}, & m = n + 1 \\ b_n, & m = n - 1 \end{cases} \quad (9)$$

Therefore the general structure of the Liouvillian matrix in terms of Krylov operator states is given by

$$(\mathcal{O}_m|\mathcal{L}|\mathcal{O}_n) = \mathcal{L}_{mn} = \begin{pmatrix} 0 & b_1 & 0 & 0 & \dots & 0 \\ b_1 & 0 & b_2 & 0 & \dots & 0 \\ 0 & b_2 & 0 & b_3 & \dots & 0 \\ \vdots & & \ddots & & \ddots & \vdots \\ & & & & \ddots & b_{\mathcal{K}-1} \\ 0 & 0 & 0 & \dots & b_{\mathcal{K}-1} & 0 \end{pmatrix} \quad (10)$$

### C. Stability of the Lanczos algorithm

The Lanczos algorithm, introduced in the previous section, is known to suffer from numerical instabilities when constructing the Krylov space. Numerical round-off error can lead to the degradation of the orthogonality between Krylov basis vectors and subsequently to unstable sequences of Lanczos coefficients  $\{b_n\}$ .

In order to reduce the numerical instability and ensure that the Krylov basis stays orthogonal, we implement the Lanczos method with full orthogonalization (FO) throughout the whole work. FO means that on every Lanczos iteration step, we orthogonalize  $A_n$  against all operator basis states already in the Krylov basis (after step 2 in the algorithm in the previous section). Since we use FO, we can also modify step 2 of the Lanczos algorithm to reduce computational time and still ensure that we get a proper ortho-normalized set of Krylov operator basis states. We now present the algorithm we used throughout this work (also see [2, 3]):

- (a) Set  $b_0 \equiv 0$  and  $\mathcal{O}_{-1} = 0$ .
- (b) For  $n \geq 1$ :  $|A_n\rangle = |\mathcal{L}\mathcal{O}_{n-1}\rangle$  where  $|A_n\rangle$  is enforced to be Hermitian since we always initiate in this work with a Hermitian operator  $|\mathcal{O}_0\rangle$  (see the text below Eq. (12)).
- (c) Full orthogonalization (FO) of  $|A_n\rangle$  against all previous  $|\mathcal{O}_i\rangle$  with  $i < n$ :  $|A_n\rangle \rightarrow |A_n\rangle - \sum_{i=0}^{n-1} |\mathcal{O}_i\rangle(\mathcal{O}_i|A_n\rangle)$ .
- (d) Set  $b_n = \sqrt{\langle A_n|A_n\rangle}$ .
- (e) Stop if  $b_n = 0$ , else set  $|\mathcal{O}_n\rangle = \frac{|A_n\rangle}{b_n}$  and jump to step 2.

This again leads to a properly ortho-normalized Krylov basis as in Eq. (7). Modifying step 2 in previous subsection to step (b) above does lead to a change of structure of the Liouvillian matrix in Eq. (10). Using this algorithm, we get as matrix elements the following:

$$\begin{aligned} \langle \mathcal{O}_m | \mathcal{L} | \mathcal{O}_n \rangle &= \langle \mathcal{O}_m | A_{n+1} \rangle \xrightarrow{FO} \langle \mathcal{O}_m | \left[ |A_{n+1}\rangle - \sum_{i=0}^n |\mathcal{O}_i\rangle(\mathcal{O}_i|A_{n+1}\rangle) \right] \\ &= \langle \mathcal{O}_m | A_{n+1} \rangle - \sum_{i=0}^n \langle \mathcal{O}_m | \mathcal{O}_i \rangle (\mathcal{O}_i | A_{n+1} \rangle) = \begin{cases} b_{n+1}, & m = n + 1 \\ 0, & \forall m \neq n + 1 \end{cases} \end{aligned} \quad (11)$$

Therefore we obtain a lower-triangular matrix for the Liouvillian matrix  $\mathcal{L}_{mn} = \langle \mathcal{O}_m | \mathcal{L} | \mathcal{O}_n \rangle$  where indices  $m$  and  $n$  label rows and columns, respectively. But we obtain the same set of Lanczos coefficients  $\{b_n\}$  as for the full Lanczos algorithm and this modified algorithm serves to make the numerical implementation more stable [2].

Next, we exploit the special structure of the Liouvillian operator  $\mathcal{L} \equiv \iota[H, \bullet]$  in the sense that this form of  $\mathcal{L}$  preserves Hermiticity when applied on any arbitrary Hermitian operator  $\mathcal{O}_h$ :

$$(\mathcal{L}\mathcal{O}_h)^\dagger = (\iota[\mathcal{H}, \mathcal{O}_h])^\dagger = -\iota(\mathcal{H}\mathcal{O}_h - \mathcal{O}_h\mathcal{H})^\dagger = \iota(-\mathcal{O}_h\mathcal{H} - (-)\mathcal{H}\mathcal{O}_h) = \mathcal{L}\mathcal{O}_h \quad (12)$$

Throughout this work, we always start with a Hermitian operator  $|\mathcal{O}_0\rangle$ . Therefore, all the Krylov operator basis states obtained through the Lanczos algorithm in Eq. (7) are—by construction—also Hermitian. Therefore all the intermediate  $\{|A_n\rangle\}$  are all Hermitian (obtained in step (b) above). We find that imposing the redundant step of re-enforcing the Hermiticity condition on the  $|A_n\rangle$  after applying the Lanczos step (step (b)) significantly improves the stability of the algorithm. Even though applying the FO on  $|A_n\rangle$  in step (c) can lead to loss of Hermiticity, we find that we *never* have to impose Hermiticity condition after the (FO) step (c). The error manifested in the overlap of the Lanczos basis continues to be negligibly small.

Next, we quantify the error analysis that we will present below. To show that all of the Krylov basis states  $\{|\mathcal{O}_n\rangle\}$  in Eq. (7) are orthogonal within acceptable accuracy, we calculate

$$\epsilon_n = \max_{i < n} \langle \mathcal{O}_i | \mathcal{O}_n \rangle, \quad (13)$$

to assess the accuracy of the sequence  $\{b_n\}$ .

We now present the accuracy of our data both for the coupled SYK model and the quantum East model by showing the maximum value of  $\epsilon_n$ . As can be seen from the provided plots in Fig. 1,  $\max_n(\epsilon_n)$  is always negligibly small. Naturally, we have also checked for other cases for all system sizes and all parameter values that we have considered in this work (including the supplemental material) and  $\epsilon_n$  remains negligibly small. From this we conclude that the *Krylov variance* can be calculated robustly for arbitrary systems without numerical instabilities.

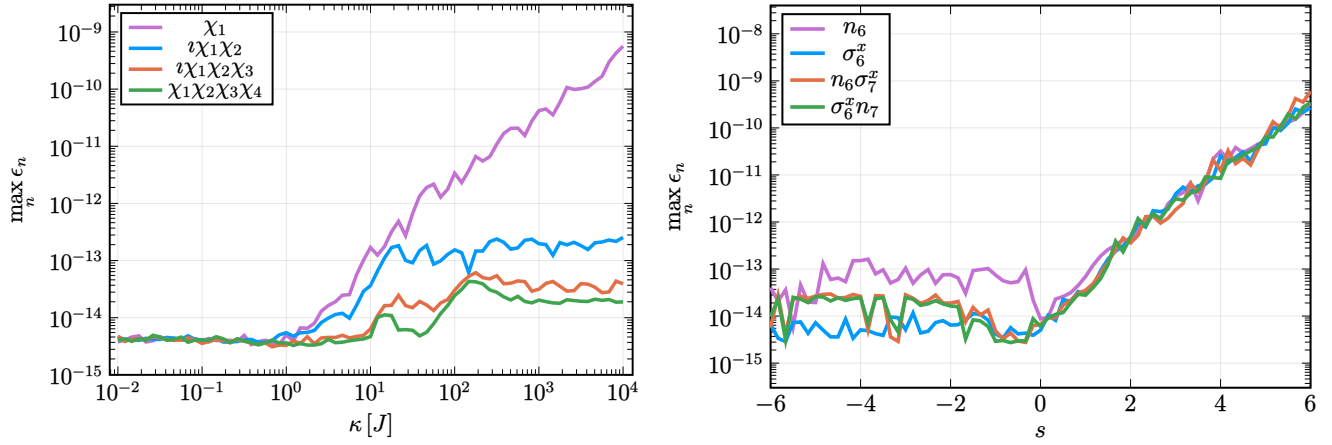


Figure 1: Graphs of the maximal overlap (maximum of Eq. (13)) in the Lanczos basis as a function of system parameter for the coupled SYK model (left) and the quantum East model (right) for all operators shown in the main manuscript for system size  $N = 26$  and  $L = 13$ , respectively. In the case of the coupled SYK model we not only take the maximum over all  $n$  but also for all realizations. The numerical stability of the operator Lanczos algorithm shown here is representative of all other plots considered in this work that we have naturally checked for.

#### D. Krylov complexity

Since we have the Krylov basis as in Eq. (7), we can expand any operator  $|\mathcal{O}(t)\rangle$  in terms of these basis states as

$$|\mathcal{O}(t)\rangle = \sum_{n=0}^{\mathcal{K}-1} \phi_n(t) |\mathcal{O}_n\rangle, \quad (14)$$

where we have  $|\mathcal{O}(t=0)\rangle = |\mathcal{O}_0\rangle$ . Here  $\phi_n(t)$  are time-dependent functions that capture the spread of the operator over different Krylov basis vectors. We now use the Heisenberg equation of motion

$$\partial_t \mathcal{O}(t) = i[\mathcal{H}, \mathcal{O}(t)] = \mathcal{L}\mathcal{O}(t) \quad (\mathcal{L} \equiv i[\mathcal{H}, \bullet]), \quad (15)$$

where we substitute Eq. (14) for  $|\mathcal{O}(t)\rangle$  to get the following differential equation for  $\phi(t)$ :

$$\partial_t \phi_n(t) = b_n \phi_{n-1}(t) + b_{n+1} \phi_{n+1}(t), \quad (16)$$

with the initial conditions  $\phi_n(t=0) = \delta_{n,0}$ ,  $b_{n=0} = 0$ , and  $\phi_{n=-1}(t) = 0$ . Therefore solving this “real-wave-equation-type” structure for  $\phi_n(t)$  is equivalent to evolving the operator  $|\mathcal{O}(t)\rangle$  (Eq. (14)). Thus the Lanczos coefficients  $\{b_n\}_{n=1}^{\mathcal{K}-1}$  are physically interpreted as “nearest-neighbor hopping amplitudes” on this one-dimensional chain with  $\phi_n(t)$  being the “wavefunction” of the moving “particle” along the chain. With this setup, the Krylov complexity (also sometimes referred to as  $K$ -complexity) is defined as

$$K(t) \equiv \sum_{n=0}^{\mathcal{K}-1} n |\phi_n(t)|^2, \quad (17)$$

which can be physically interpreted as expectation value of “position” on the above Krylov chain. It can be easily verified that if we use a different expansion coefficient in Eq. (14) such as

$$|\mathcal{O}(t)\rangle = \sum_{n=0}^{\mathcal{K}-1} i^n \psi_n(t) |\mathcal{O}_n\rangle \quad (18)$$

and use the Heisenberg’s equation of motion for  $|\mathcal{O}(t)\rangle$  in Eq. (15), we get the following differential equation for  $\psi_n(t)$ :

$$i\partial_t \psi_n(t) = b_n \psi_{n-1}(t) - b_{n+1} \psi_{n+1}(t), \quad (19)$$

which has a “Schrödinger-type” structure and the same initial conditions as before, namely  $\psi_n(t=0) = \delta_{n,0}$ ,  $b_{n=0} = 0$ , and  $\psi_{n=-1}(t) = 0$ . The coefficients  $\phi_n(t)$  and  $\psi_n(t)$  are related through  $\phi_n(t) = i^n \psi_n(t)$ .

## E. Growth of Krylov complexity

For a chaotic system, we now analyze the various stages of growth of Krylov complexity. We proceed in chronological dynamical order to form a complete picture.

### 1. Universal Operator Growth Hypothesis

A “universal operator growth hypothesis” was proposed in [4] whose fundamental tenet is that any chaotic system implies a linear growth of Lanczos coefficients  $\{b_n\}$  with  $n$ , or in other words  $b_n \sim \alpha n$  (with logarithmic corrections in one dimension [4]) where the proportionality  $\alpha$  is system dependent. It was shown [4] that  $b_n \sim \alpha n$  implies an exponential growth of Krylov complexity defined in Eq. (17) as  $K(t) \sim e^{2\alpha t}$  and that  $\alpha$  bounds the Lyapunov exponent as  $\lambda_L \leq 2\alpha$ . This is an improvement over the famous Maldacena-Shenker-Stanford bound on chaos [5] (see Fig. 8 of [4] for the case of large- $q$  SYK model).

### 2. Random matrix theory

Operator growth hypothesis as mentioned above deals with the initial growth of operators where the Lanczos coefficients  $b_n$  grows with  $n$  [6]. In the context of random matrix theory (RMT), the asymptotic value of  $b_n$  in large- $N$  theories saturates to 1. In other words,

$$\lim_{n \rightarrow \infty} \lim_{N \rightarrow \infty} b_n = 1 \quad (\text{RMT}) \quad (20)$$

We know that eigenvalues of quantum many-body chaotic systems are extensive in the degrees of freedom of the system while the eigenvalues for a random matrix Hamiltonian is usually scaled to be of  $\mathcal{O}(1)$ . That’s why in order to compare the growth of operators with the random matrix behavior, we need to properly scale our results using the fact that the energy scale is conjugate to the time scale.

The spectrum of a random matrix can be described by a semi-circle of width two and the non-re-scaled Lanczos coefficients are subject to the same scale as the eigenvalues. Therefore, we re-scale the original Lanczos coefficients  $\tilde{b}_n$  with respect to the largest and smallest eigenvalues  $E_{\max}$  and  $E_{\min}$  by

$$b_n = \tilde{b}_n / r_{\text{spectrum}}, \quad \text{where} \quad r_{\text{spectrum}} = \frac{E_{\max} - E_{\min}}{2}. \quad (21)$$

This ensures that the Lanczos coefficients  $b_n$ —as shown throughout the main manuscript and the supplementary material—are all re-scaled in such a way that they are comparable with the results of RMT allowing for their proper comparison throughout the parameter space. Indeed, this process resembles re-scaling of the Hamiltonian to energy scales of the original Wigner semi-circle law for random matrices.

### 3. Decay at the edge of Krylov space

At the edge of the Krylov space [2], the Lanczos coefficients  $\{b_n\}$  descent back to zero where the algorithm stops and this signifies the saturation of the Krylov complexity.

### 4. Summary

Therefore the picture that emerges for the growth of Krylov complexity and its mapping to the Krylov space in terms of the Lanczos coefficients  $\{b_n\}$  has three stages where the third stage kicks in after a significantly long time as mentioned below. The three stages are [2, 7, 8]

1. initially a linear growth of  $\{b_n\}$  for  $\ll n < \mathcal{O}(f)$  implies an exponential growth in time of  $K(t)$  for  $0 \lesssim t < \mathcal{O}(\log(f))$ ,
2. a saturation after the linear growth happens for  $\{b_n\}$  for  $n \gg \mathcal{O}(f)$  that implies a linear-in-time growth of  $K(t)$  for  $t \gtrsim \mathcal{O}(\log(f))$ , and

3. finally the descent of  $\{b_n\}$  to zero for  $n \sim \mathcal{O}(e^{2f})$  implying a saturation of  $K(t)$  for  $t \sim \mathcal{O}(e^{2f})$ .

We argued in this work that all local operators loses their sense of locality once the stage (2) of the growth kicks in and that's why this allows for a possibility to have universal behavior for all operators (with vanishing overlap with any other conserved quantity in the system).

### F. Krylov chain

As argued in [1], the integrability of a system suppresses the  $K$ -complexity and this can be mapped onto the phenomenology of Anderson localization on the Krylov chain. The reason for this mapping to work, as we will also show below, is that there is a larger variance of the Lanczos coefficients  $\{b_n\}$  which implies a stronger disorder in hopping amplitudes on the Krylov chain. Therefore integrability enhances localization on the Krylov chain where the localization length is given by [1, 9]  $l_{\text{loc}} \propto \sqrt{\mathcal{K}}/\sigma$  where  $\mathcal{K}$  is the length of the Krylov chain and  $\sigma$  is defined as

$$\sigma^2 = \text{Var}(x_j) \quad \text{where} \quad x_j \equiv \ln\left(\frac{b_{2j-1}}{b_{2j}}\right). \quad (22)$$

This measure of the localization length is our suggested probe in this work for capturing weak ergodicity-breaking after the scrambling time (stage 2 of the  $K$ -complexity growth).

We argue that due to the vast size of the operator Hilbert space  $\mathcal{N}^2 - \mathcal{N} - 1$ ,  $\sigma^2$  will always be dominated by the dynamics after the ramp of the Lanczos coefficients  $\{b_n\}$ . Therefore, we ignore the initial ramp of  $\{b_n\}$  and focus on the large  $j$  statistics of  $\{x_j\}$ . However, the short-time dynamics on the Krylov chain are still relevant for the chaotic behavior of the system which is also captured on the Krylov chain as the scrambling time has yet not been reached. This is also the domain of the ‘‘universal operator growth hypothesis’’ [4]. Therefore, we show the analysis of  $\sigma^2$  also for the entire sequence of  $\{b_n\}$  here in the supplementary material (Fig. 6(a), Fig. 6(b), Fig. 9). However, these plots are only qualitative in nature, the full quantitative prediction of the point of weak ergodicity-breaking transition can be deduced from the plots where the Lanczos coefficients are considered only after the scrambling time. The reason is grounded in loss of notion of locality as explained above as well as in the main manuscript.

### G. Equivalence of different approaches

In the literature on Krylov complexity, there is another physically equivalent definition of Liouvillian is used which is given by

$$\tilde{\mathcal{L}} \equiv [\mathcal{H}, \bullet], \quad (23)$$

in contrast to our definition of Liouvillian considered throughout this work, namely  $\mathcal{L} \equiv i[\mathcal{H}, \bullet]$ . We now show equivalence between these two approaches. We always initialize the Lanczos algorithm with a Hermitian operator  $|\mathcal{O}_0\rangle$ . As we showed in Eq. (12) that  $\mathcal{L}$  preserves Hermiticity, this is not true for  $\tilde{\mathcal{L}}$  which acts on any arbitrary Hermitian operator  $\mathcal{O}_h$  to give an anti-Hermitian operator  $\mathcal{O}_{ah}$  and *vice versa*:

$$\begin{aligned} (\tilde{\mathcal{L}}\mathcal{O}_h)^\dagger &= ([\mathcal{H}, \mathcal{O}_h])^\dagger = (\mathcal{H}\mathcal{O}_h - \mathcal{O}_h\mathcal{H})^\dagger = (\mathcal{O}_h\mathcal{H} - \mathcal{H}\mathcal{O}_h) = -\tilde{\mathcal{L}}\mathcal{O}_h \\ (\tilde{\mathcal{L}}\mathcal{O}_{ah})^\dagger &= ([\mathcal{H}, \mathcal{O}_{ah}])^\dagger = (\mathcal{O}_{ah}^\dagger\mathcal{H} - \mathcal{H}\mathcal{O}_{ah}^\dagger) = (-\mathcal{O}_{ah}\mathcal{H} + \mathcal{H}\mathcal{O}_{ah}) = \tilde{\mathcal{L}}\mathcal{O}_{ah} \end{aligned} \quad (24)$$

Therefore when the Lanczos algorithm, as explained in Sec. IB, is implemented using  $\tilde{\mathcal{L}}$  instead of  $\mathcal{L}$  by starting from an initial Hermitian operator  $|\mathcal{O}'_0\rangle$ , we get the Krylov basis states as  $\{|\mathcal{O}'_n\rangle\}_{n=0}^{\mathcal{K}-1}$  which are alternating between Hermitian (for even values of  $n$ ) and anti-Hermitian (for odd values of  $n$ ) operator states. Therefore  $i^n\mathcal{O}'_n$  is Hermitian for all values of  $n$ . Moreover, for both  $\mathcal{L}$  and  $\tilde{\mathcal{L}}$ , the diagonal elements in the Liouvillian matrix representation are identically zero. This is because  $(\mathcal{O}'_n|\tilde{\mathcal{L}}|\mathcal{O}'_n) = 0$  irrespective of whether  $|\mathcal{O}'_n\rangle$  is Hermitian or anti-Hermitian. Recall the definition of inner-product:  $(A|B) = \frac{1}{\mathcal{N}} \text{Tr}[A^\dagger B]$  where  $\mathcal{N}$  is the dimension of the Hilbert space. Let the off-diagonal Lanczos elements be  $\{b_n\}$  and  $\{b'_n\}$  which are obtained through  $\mathcal{L}$  and  $\tilde{\mathcal{L}}$ , respectively. Both  $\mathcal{L}$  and  $\tilde{\mathcal{L}}$  have a tri-diagonal matrix representation (Eq. (10)) in  $\{b_n\}$  and  $\{b'_n\}$ , respectively which can be written as ( $\mathcal{K}$  is the dimension of the Krylov space)

$$\mathcal{L} = \sum_{n=0}^{\mathcal{K}-2} b_{n+1} (|\mathcal{O}_n\rangle\langle\mathcal{O}_{n+1}| + |\mathcal{O}_{n+1}\rangle\langle\mathcal{O}_n|), \quad \tilde{\mathcal{L}} = \sum_{n=0}^{\mathcal{K}-2} b'_{n+1} (|\mathcal{O}'_n\rangle\langle\mathcal{O}'_{n+1}| + |\mathcal{O}'_{n+1}\rangle\langle\mathcal{O}'_n|). \quad (25)$$

In order to understand the connection between the two approaches, we study the evolution of an arbitrary operator with respect to both  $\mathcal{L}$  (already shown in Eq. (3) and reproduced here for convenience) and  $\tilde{\mathcal{L}}$

$$|\mathcal{O}(t)\rangle = e^{\mathcal{L}t}|\mathcal{O}_0\rangle = \sum_{n=0}^{\infty} \frac{t^n}{n!} |\mathcal{L}^n \mathcal{O}_0\rangle, \quad |\mathcal{O}'(\tau)\rangle = e^{i\tilde{\mathcal{L}}\tau}|\mathcal{O}'_0\rangle = \sum_{n=0}^{\infty} \frac{(i\tau)^n}{n!} |\tilde{\mathcal{L}}^n \mathcal{O}'_0\rangle, \quad (26)$$

where time is labeled by  $t$  and  $\tau$  to denote the time evolution by  $\mathcal{L}$  and  $\tilde{\mathcal{L}}$  respectively. Since any operator matches at initial time  $t = \tau = 0$ , namely  $|\mathcal{O}(t=0)\rangle = |\mathcal{O}'(\tau=0)\rangle$ , this implies for  $n = 0$  Krylov operator basis state that  $|\mathcal{O}_0\rangle = |\mathcal{O}'_0\rangle$  which, for instance, is used as an initial operator in the Lanczos algorithm either using  $\mathcal{L}$  or  $\tilde{\mathcal{L}}$ . Therefore, assuming analytic continuation, we find equivalence between the two definitions using the mapping  $\{t \leftrightarrow i\tau, \mathcal{L} \leftrightarrow \tilde{\mathcal{L}}\}$  which ensures that the physical content stays the same. For instance, the Heisenberg's equation of motion in Eq. (15) structurally remains the same under this transformation where we take  $t \rightarrow i\tau$  and  $\mathcal{L} \rightarrow \tilde{\mathcal{L}}$  as well as denote  $\mathcal{O}(t \rightarrow i\tau) = \mathcal{O}'(\tau)$ .

We know that the evolution of operator in Eq. (26) can be translated to a differential equation of ‘‘wave-equations’’ on a one-dimensional Krylov chain (e.g., Eq. (16) corresponding to Eq. (14), or equivalently Eq. (19) corresponding to Eq. (18)). Similarly we expand an arbitrary operator in terms of Krylov basis operator states  $\{|\mathcal{O}'_n\rangle\}_{n=0}^{\mathcal{K}-1}$  corresponding to the evolution through  $\tilde{\mathcal{L}}$ :

$$|\mathcal{O}'(\tau)\rangle = \sum_{n=0}^{\mathcal{K}-1} \varphi_n(\tau) |\mathcal{O}'_n\rangle \quad (27)$$

Then the Heisenberg equation of motion leads to the following ‘‘Schrödinger-type’’ differential equation corresponding to operator growth with respect to  $\tilde{\mathcal{L}}$ :

$$i\partial_\tau \varphi_n(\tau) = -b'_{n+1} \varphi_{n+1}(\tau) - b'_n \varphi_{n-1}(\tau), \quad (28)$$

with the initial conditions  $\varphi_n(\tau=0) = \delta_{n,0}$ ,  $b'_{n=0} = 0$  and  $\varphi_{n=-1}(\tau) = 0$ . Here we used the Lanczos step  $|\tilde{\mathcal{L}}\mathcal{O}'_n\rangle = b'_{n+1}|\mathcal{O}'_{n+1}\rangle + b'_n|\mathcal{O}'_{n-1}\rangle$ . This is the same differential equation as found in [6] using  $\tilde{\mathcal{L}}$ . If we translate this differential equation using the aforementioned mapping and denote  $\varphi_n(\tau \rightarrow -it) = \phi(t)$ , then we re-derive our ‘‘real-wave-equation-type’’ differential equation in Eq. (16) along with the same initial conditions where we have used  $\mathcal{L}$  for operator evolution. Therefore the mapping obtained here also ensures that the Lanczos coefficients corresponding to  $\mathcal{L}$  and  $\tilde{\mathcal{L}}$  are mapped onto each other thereby proving the equivalence of the two approaches. As a redundant check, we express an arbitrary operator using another set of expansion coefficients (like Eq. (18)) as

$$|\mathcal{O}'(\tau)\rangle = \sum_{n=0}^{\mathcal{K}-1} i^n \Psi_n(\tau) |\mathcal{O}'_n\rangle, \quad (29)$$

which leads to the following ‘‘real-wave-equation-type’’ differential equation

$$\partial_\tau \Psi(\tau) = -b'_{n+1} \Psi_{n+1}(\tau) + b'_n \Psi_{n-1}(\tau), \quad (30)$$

with the initial conditions  $\Psi_n(\tau=0) = \delta_{n,0}$ ,  $b'_{n=0} = 0$  and  $\Psi_{n=-1}(\tau) = 0$ . This is the same as obtained in [4, 6] using  $\tilde{\mathcal{L}}$ . We again re-derive ‘‘Schrödinger-type’’ differential equation in Eq. (19) when we use the aforementioned mapping where we denote  $\Psi(\tau \rightarrow -it) = \psi(t)$ . Therefore, we again found that the Lanczos coefficients corresponding to  $\mathcal{L}$  and  $\tilde{\mathcal{L}}$  are mapped one-to-one using the mapping. Hence we have established that the physical content of both the approaches corresponding to  $\mathcal{L}$  and  $\tilde{\mathcal{L}}$  are equivalent and can be mapped onto each other using the aforementioned mapping.

## II. COUPLED SACHDEV-YE-KITAEV MODEL

The Hamiltonian considered in the main manuscript is

$$\mathcal{H} = \frac{2}{\sqrt{N}} \sum_{1 \leq i < j < k < l \leq N} J_{ijkl} \chi_i \chi_j \chi_k \chi_l + i \sum_{1 \leq i < j \leq N} \kappa_{ij} \chi_i \chi_j. \quad (31)$$

The random couplings  $J_{ijkl}$  and  $\kappa_{ij}$  are drawn from a Gaussian distribution with variance  $\frac{6J^2}{N^3}$  and  $\frac{\kappa^2}{N}$  respectively, where  $J$  and  $\kappa$  are system parameters and we take the large- $N$  limit [10]. We measure  $\kappa$  in units of  $J$  where we

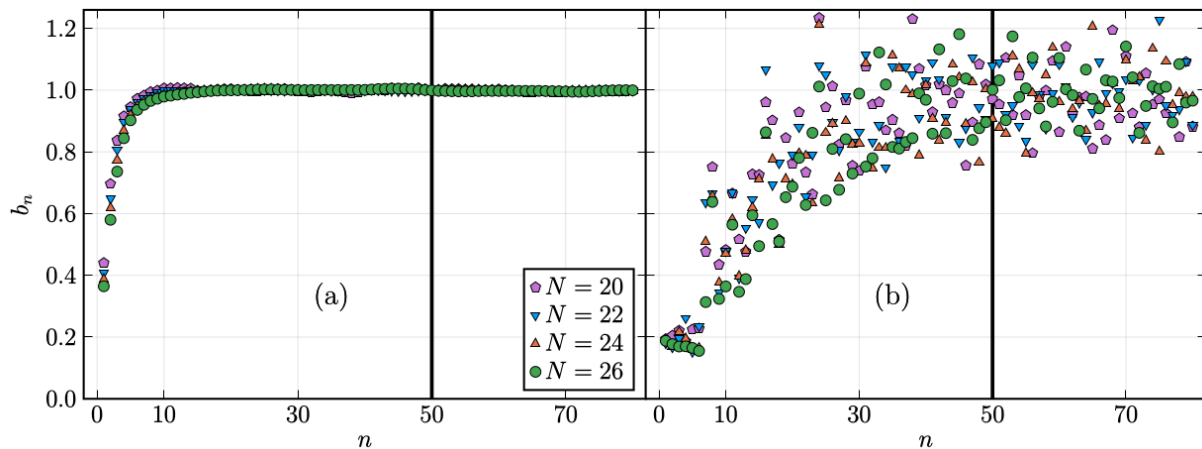


Figure 2: Lanczos coefficients  $\{b_n\}$  compared for different system sizes for the coupled SYK model (Eq. (31)) in (a) the ergodic regime  $\kappa = 0.01 J$  and in (b) the ergodicity-broken regime  $\kappa = 100 J$  with the initial operator  $|\mathcal{O}_0\rangle = \chi_1$  at  $N = 26$ . We visualize the end of the ramp for all parameters considered with a vertical solid line at  $n = 50$ .

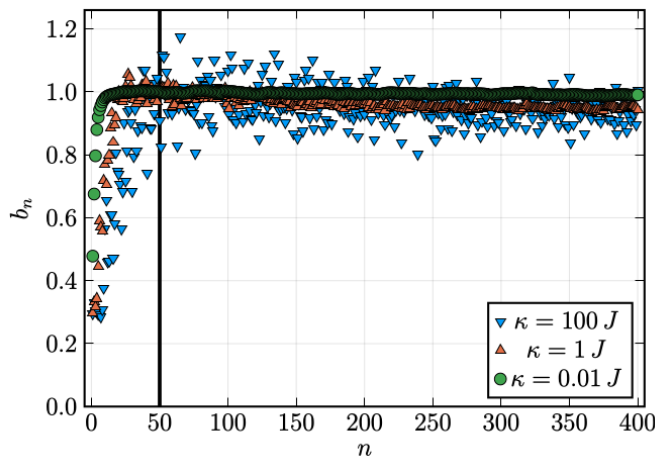


Figure 3: Lanczos coefficients  $\{b_n\}$  at  $\beta = 0$  for the coupled SYK model (31) for  $N = 26$ . The initial operator is  $|\mathcal{O}_0\rangle = \nu\chi_1\chi_2$  which—in contrast to  $\chi_1$ —has support in only a single charge parity sector. Again, we mark the value of  $n = 50$  where the initial ramp in the Lanczos coefficients stops with a solid vertical line.

have kept  $J = 1$  to fix the unit system. This is the same Hamiltonian as studied in [11] where they studied the adiabatic gauge potential (AGP) and found a delayed thermalization due to the violation of ETH scaling in the AGP as confirmed by the spectral form factor analyses.

The coupled SYK system needs to be averaged over disorder realizations due to the presence of random couplings. We have averaged  $\sigma$  over multiple realizations and then plot the Krylov variance denoted by  $(\bar{\sigma})^2$ . The reason we average over  $\sigma$  instead of  $\sigma^2$  is that the standard deviation  $\sigma$  directly measures the inverse localization length on the Krylov chain, given by  $l_{\text{loc}} \propto \sqrt{\mathcal{K}}/\sigma$ . Here  $\mathcal{K}$  is the length of the Krylov chain. Therefore, conceptually speaking,  $\sigma$  is a quantity of interest on the Krylov chain.

The Majorana SYK has a particle-hole symmetry as well as charge-parity symmetry. We formalize this now. For  $N$  Majorana fermions, the dimension of the Hilbert space is  $2^{N/2}$  which is equivalent to having  $L = N/2$  Dirac fermions. Often, it is convenient to use the Dirac basis to computationally handle Majorana fermions. Let the Dirac operators be denoted by  $c_j$  where  $j = 1, 2, \dots, L$  where  $L = N/2$ . They satisfy the standard anti-commutation relations:  $\{c_i, c_j^\dagger\} = \delta_{ij}$ ,  $\{c_i, c_j\} = 0$  and  $\{c_i^\dagger, c_j^\dagger\} = 0$ . Then the Majorana fermions can be written as [12]

$$\chi_{2j} = \frac{c_j + c_j^\dagger}{\sqrt{2}}, \quad \chi_{2j-1} = \frac{\imath(c_j - c_j^\dagger)}{\sqrt{2}}. \quad (32)$$

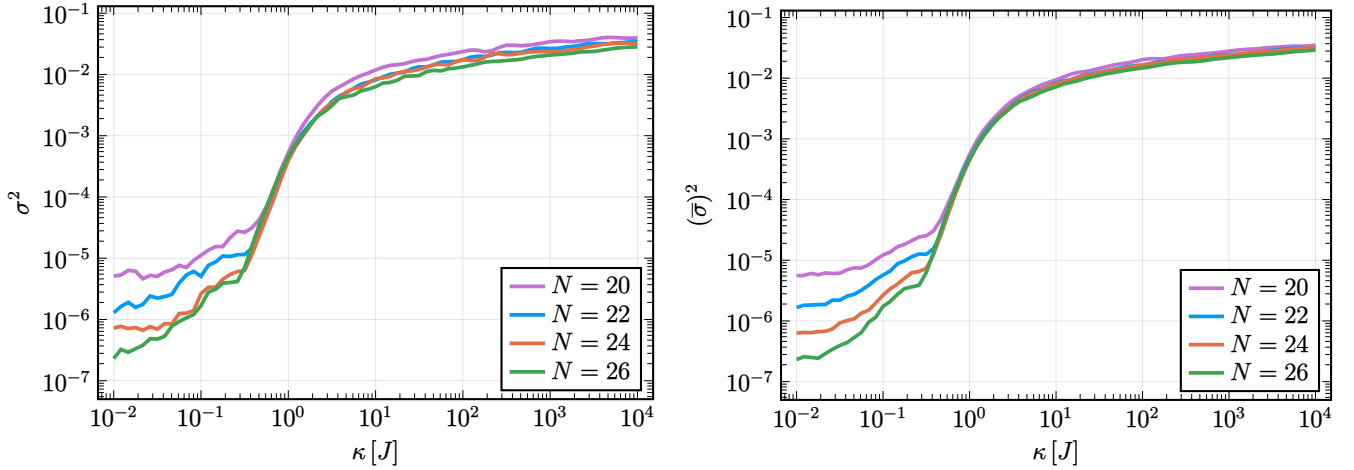


Figure 4: Plotting the Krylov variance  $\sigma^2$  against  $\kappa$  at  $\beta = 0$  for the coupled SYK model (Eq. (31)) ignoring the first 50 Lanczos coefficients  $\{b_n\}$  where  $|\mathcal{O}_0\rangle = \chi_1$  is used. On the left, we show  $\sigma^2$  for a single realization of the SYK model while on the right, we have calculated the average  $\bar{\sigma}$  from a total of 5 realizations before calculating  $(\bar{\sigma})^2$ . The plot on the right is the same plot shown in the main manuscript which we again show here for comparison.

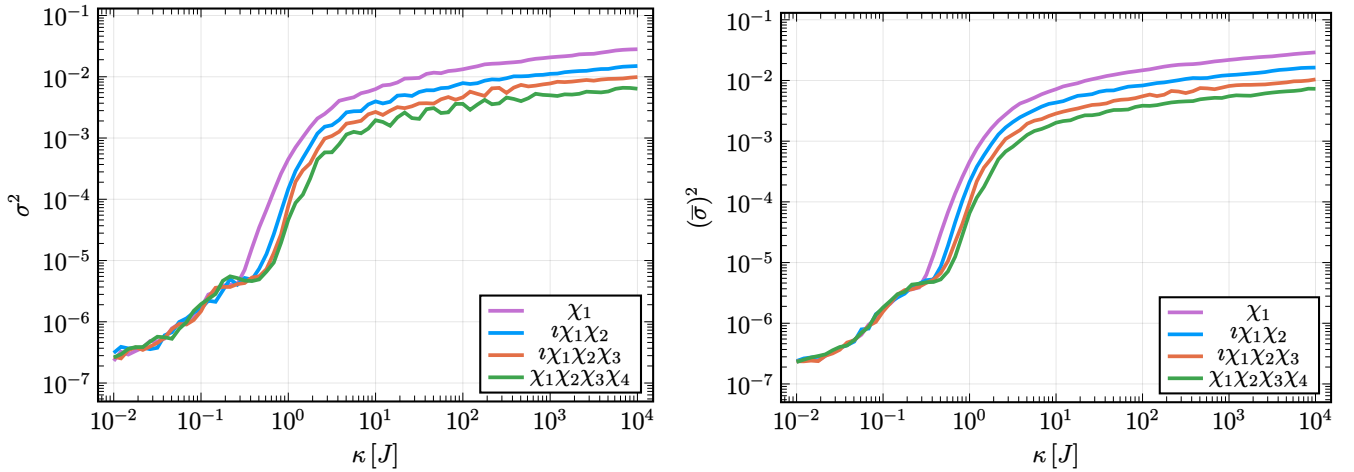


Figure 5: Plotting the Krylov variance  $\sigma^2$  against  $\kappa$  at  $\beta = 0$  for the coupled SYK model (Eq. (31)) for  $N = 26$  ignoring the first 50 Lanczos coefficients  $b_n$  for different initial operators  $|\mathcal{O}_0\rangle$ . On the left, we show  $\sigma^2$  for a single realization of the SYK model while on the right, we have calculated the average  $\bar{\sigma}$  from a total of 5 realizations before calculating  $(\bar{\sigma})^2$ . The plot on the right is the same plot shown in the main manuscript which we again show here for comparison.

Then, we can define the total charge of the system as  $Q = \sum_{j=1}^{L=N/2} c_j^\dagger c_j$ . Clearly,  $[\mathcal{H}_q, Q] \neq 0$  where  $\mathcal{H}_q$  is the Hamiltonian of single arbitrary  $q$  body Majorana SYK model where  $q$  is always considered to be even. It is given by  $\mathcal{H}_q = i^{q/2} \sum_{1 \leq i_1 < \dots < i_q \leq N} J_{i_1 \dots i_q} \chi_{i_1} \dots \chi_{i_q}$  as also mentioned in the main manuscript. Therefore the charge is not conserved but  $(Q \bmod (q/2))$  commutes with the Hamiltonian  $\mathcal{H}_q$ . For our case  $q = 4$ , therefore  $(Q \bmod 2)$  commutes with  $\mathcal{H}_4$  and therefore, the Hamiltonian  $\mathcal{H}_4$  is divided into two blocks: even sector and odd sector corresponding to even and odd values of  $Q$ . Two choices of initial operators, namely  $\chi_1$  and  $i\chi_1\chi_2\chi_3$ , have support in both symmetry sectors and in order to be consistent, we have considered the full spectrum for all operators, to generate the plots presented in the main manuscript and here in the supplemental material.

As a side remark, the symmetry between holes and particles are captured by the operator  $\hat{P} = T \prod_{j=1}^{L=N/2} (c_j + c_j^\dagger)$



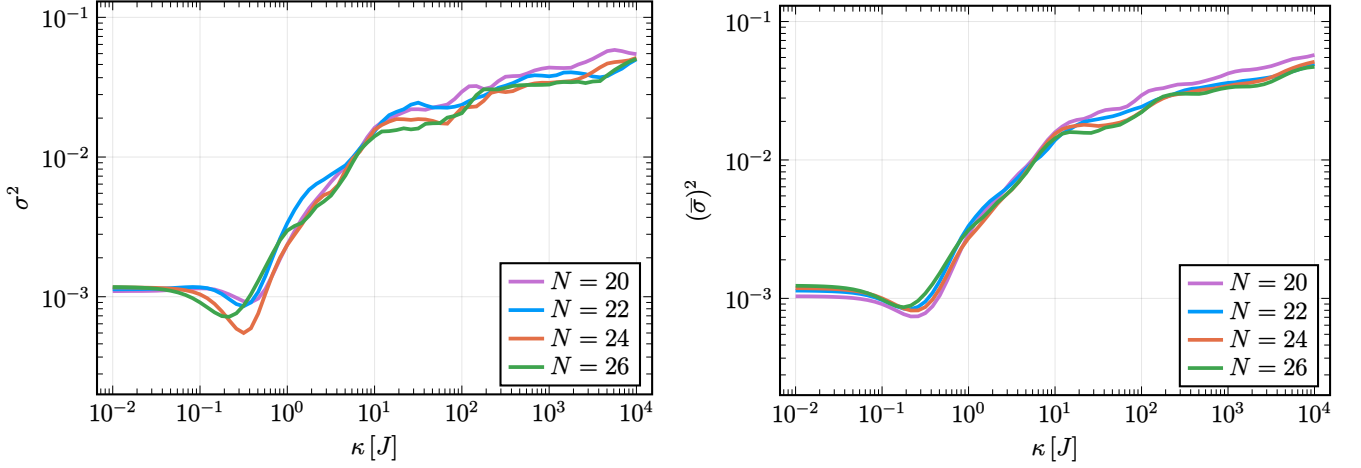


Figure 6: Plotting the Krylov variance  $\sigma^2$  against  $\kappa$  at  $\beta = 0$  for the coupled SYK model (Eq. (31)) including *all* the Lanczos coefficients  $\{b_n\}$  where  $|\mathcal{O}_0\rangle = \chi_1$  is used. On the left, we show  $\sigma^2$  for a single realization of the SYK model while on the right, we have calculated the average  $\bar{\sigma}$  from a total of 5 realizations before calculating  $(\bar{\sigma})^2$ . We still observe a qualitative change in behavior around the point of weak ergodicity-breaking as observed in Fig. 4 above or Fig. 2 of the main manuscript by using our prescription.

where  $T : \mathbb{C} \rightarrow \mathbb{C}$  such that  $Tz = \bar{z}$  (complex conjugate)  $\forall z \in \mathbb{C}$ . For  $q = 4$ ,  $\hat{P}^2 = +1$  for  $L \bmod 4 = 0, 1$  while  $\hat{P}^2 = -1$  for  $L \bmod 4 = 2, 3$ . Using the relation  $\hat{P}c_j\hat{P} = \alpha c_j^\dagger$  and  $\hat{P}c_j^\dagger\hat{P} = \alpha c_j$ , we get  $\hat{P}\chi_j\hat{P} = \alpha\chi_j$  where  $\alpha \equiv (-1)^{L-1}\hat{P}^2$ . Using all these properties, one can show that  $[\mathcal{H}_4, \hat{P}] = 0$  and hence is a symmetry of the Hamiltonian. Generalization to  $q$ -body case is straightforward.

In Fig. 1 of the main manuscript, we showed the Lanczos coefficients corresponding to the operator  $\chi_1$  for  $N = 26$ , here we show in Fig. 2 the coefficients for different system sizes in the ergodic and ergodic-broken regimes. We also show in Fig. 3 the Lanczos coefficients for another operator  $|\mathcal{O}_0\rangle = \nu\chi_1\chi_2$  for a given system size which has a support in both symmetry sectors of the Hamiltonian as explained above. Both the plots show that our cut-off  $n = 50$  for the initial ramp holds across all considered system sizes. We have also checked for all combinations of operators and system sizes to ensure the validity of the cut-off.

Next we show the Krylov variance  $\sigma^2$  plotted against  $\kappa$  in Fig. 4 for a single realization as well as for multiple realizations of the SYK model. We can observe that a single realization shows similar features as the averaged-over-multiple-realization case which legitimizes our averaging procedure over  $\sigma$  to calculate  $(\bar{\sigma})^2$ .

In Fig. 5, we show the universality across different operators for a given system size by considering the Lanczos coefficients after the scrambling time. We again compare the results of a single realization against multiple realizations and we find a decent agreement between the two. In general we have found that the single realization case is already quite a good approximation to the case where we have averaged over multiple realizations.

The early Lanczos coefficients  $\{b_n\}$  in the initial ramp control the early time dynamics on the Krylov chain. Therefore, even though we expect universality across operators for a given system size only after the scrambling has happened, the full  $\sigma^2$  may still give insight into the short-time dynamics of the initial state on the Krylov chain. Fig. 6 shows  $(\bar{\sigma})^2$  calculated using the *full* sequence of  $\{b_n\}$  analogous to how we detect the weak ergodicity-transition in the main manuscript. We again see a qualitative change in behavior around the transition point but—in contrast to the results in the main manuscript—we cannot use this to make a quantitative prediction about the point of weak ergodicity-breaking transition. We can also see that in the ergodic regime, there is already a difference of  $\sim 10^3$  order of magnitude when comparing Fig. 6 with Fig. 5 for the largest system size  $N = 26$ . This reinforces our claim from the main manuscript that a universal quantitative probe for weak ergodicity-breaking should be realized after the scrambling in a system has already happened.

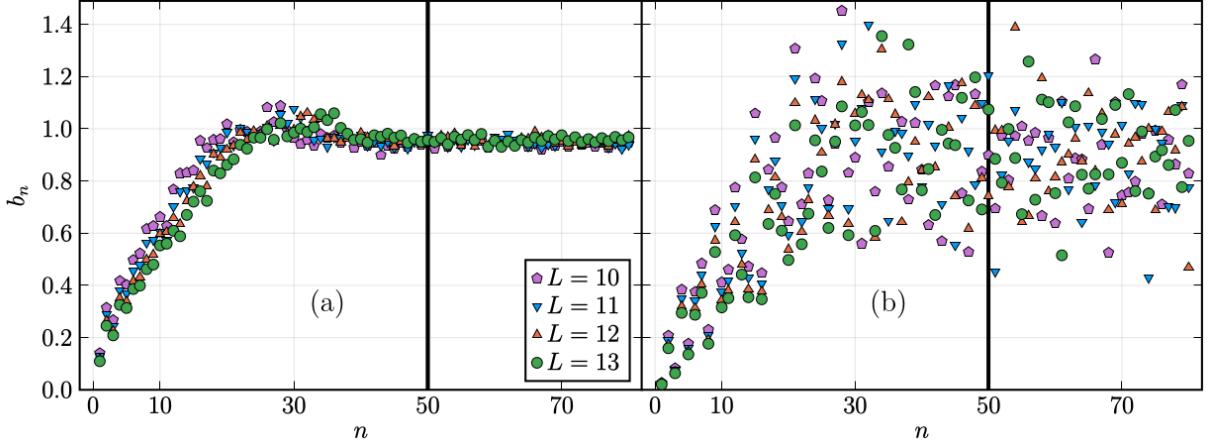


Figure 7: Lanczos coefficients  $\{b_n\}$  compared for different system sizes for the quantum East model (Eq. (33)) in (a) the ergodic regime  $s = -2$  and in (b) the ergodicity-broken regime  $s = 2$  for the initial operator  $|\mathcal{O}_0\rangle = n_6$  at  $L = 13$ . We visualize the end of the ramp with a vertical solid line at  $n = 50$ .

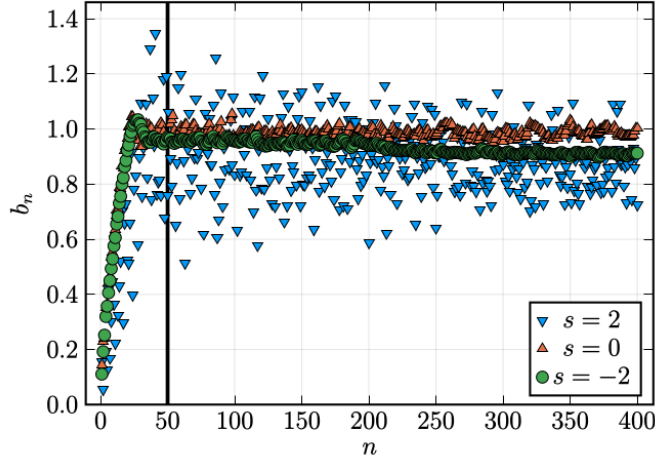


Figure 8: Lanczos coefficients  $\{b_n\}$  at  $\beta = 0$  in the quantum East model (Eq. (33)) for  $L = 13$ . The initial operator is  $|\mathcal{O}_0\rangle = \sigma_6^x$ . We again mark the value of  $n = 50$  where the ramp in the Lanczos coefficients ends by a solid vertical line.

### III. QUANTUM EAST MODEL

The Hamiltonian of the Quantum East model as defined on a 1D lattice of size  $L$  is [13]

$$\mathcal{H} = -\frac{1}{2} \sum_{i=1}^{L-1} n_i (e^{-s} \sigma_{i+1}^x - \mathbb{1}), \quad (33)$$

where  $n_i$  is the projection on the spin-up state at lattice site  $i$ ,  $\sigma_i^x$  is the  $x$ -Pauli operator acting on that respective lattice site  $i$  and  $s$  is a system parameter. As  $n_i$  projects on the spin-up state, we can consider any spin-down lattice site as a kinetic constraint for dynamics on the next lattice site.

Naturally, due to the kinetic constraint, the quantum East model as in Eq. (33) can be divided into symmetry sectors: as spin-up sites can not facilitate dynamics on the previous lattice sites, a string of  $l$  spin-down lattice sites, starting on the first site, will be kinetically disconnected from the dynamical part of the system. Therefore, their states must also be disconnected in Fock space, giving rise to a block structure of the Hamiltonian with the quantum number  $l$ .

As all of these symmetry blocks are self-similar—in the sense that they just represent the same system but with a smaller system size—we naturally only want to study the largest symmetry block. To maximize the number of

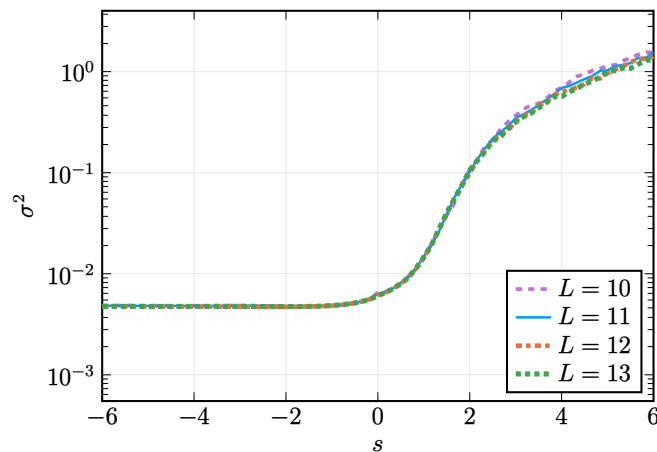


Figure 9: Plotting the Krylov variance  $\sigma^2$  at  $\beta = 0$  for the quantum East model (Eq. (33)) for different system sizes where we have considered *all*  $b_n$  for the calculation of  $\sigma^2$ . The initial operator in the Lanczos iteration is  $|\mathcal{O}_0\rangle = n_{\lfloor L/2 \rfloor}$ . We can still observe a small qualitative change in behavior around  $s = 0$  which is the point of weak ergodicity-breaking (compare with Fig. 4 of the main manuscript).

dynamical sites in our computational basis we modify the boundary conditions of the Hamiltonian (33) by inserting a spin-up lattice site on the  $0^{\text{th}}$  lattice site (not simulated) and also allow for dephasing due to facilitation of dynamics on a lattice site at  $L+1$  (also not simulated). The effective Hamiltonian with the aforementioned boundary conditions can be realized as

$$\mathcal{H} = -\frac{1}{2}(e^{-s}\sigma_1^x - \mathbb{1}) - \frac{1}{2}\sum_{i=1}^{L-1}n_i(e^{-s}\sigma_{i+1}^x - \mathbb{1}) - \frac{1}{2}n_L(e^{-s} - 1). \quad (34)$$

It was shown in [13] that by modifying the regular quantum East Hamiltonian in Eq. (33) like shown above, the system's first order transition can be captured by a sharp delocalization ( $s < 0$ )/localization ( $s > 0$ ) transition in the ground-state at  $s = 0$ . Furthermore, it was shown how in the regime  $s > 0$ , localized eigenstates can be constructed at arbitrary energy density. Due to this clear picture how we can understand the dynamics in the regime  $s > 0$ , we consider a quantum East Hamiltonian with the boundaries Eq. (34) instead of Eq. (33) throughout the main manuscript.

In Fig. 3 of the main manuscript, we showed the plot for the Lanczos coefficient for the operator  $n_6$  for system size  $L = 13$ . Here we show for different system sizes the same plot for ergodic and ergodicity-broken regimes in Fig. 7. This shows that our cut-off  $n = 50$  for the initial ramp holds across all considered system sizes. Next we show the Lanczos coefficients for the operator  $\sigma_6^x$  at system size  $L = 13$  in Fig. 8. This shows that also for different operators the chosen cut-off  $n = 50$  is valid. Naturally, we have also checked for all other combinations of operators and system sizes to confirm the validity of the cut-off.

In Fig. 4 of the main manuscript, we showed the Krylov variance  $\sigma^2$  by considering the Lanczos coefficients after the cut-off. Since the early ramp of  $\{b_n\}$  does capture the early-time dynamics on the Krylov chain, we also show the Krylov variance including all the Lanczos coefficients  $\{b_n\}$  starting from  $n = 1$  in Fig. 9. We insist that although there seems to be a perfect collapse, conceptually it only makes sense to consider the Lanczos coefficients after scrambling has happened because only then the operators admit a universal description by losing their respective notion of local behavior. Note also that in the ergodic regime there is a factor of  $\sim 10^2$  difference between  $\sigma^2$  with and without using the full  $\{b_n\}$  while the saturation for ergodicity-broken regime remains the same. Therefore, there is an acute sensitivity between the two regimes when we only consider the Lanczos coefficients after the scrambling time. Hence we conclude that the analysis of the *full*  $\{b_n\}$  leads to a qualitative instead of a quantitative probing of the weak ergodicity-breaking.

---

[1] E. Rabinovici, A. Sánchez-Garrido, R. Shir, and J. Sonner, Krylov localization and suppression of complexity, *J. High Energy Phys.* **2022** (3), 1.

- [2] E. Rabinovici, A. Sánchez-Garrido, R. Shir, and J. Sonner, Operator complexity: a journey to the edge of Krylov space, *J. High Energy Phys.* **2021** (6), 1.
- [3] A. Bhattacharyya, D. Ghosh, and P. Nandi, Operator growth and Krylov complexity in Bose-Hubbard model, *J. High Energy Phys.* **2023** (12), 1.
- [4] D. E. Parker, X. Cao, A. Avdoshkin, T. Scaffidi, and E. Altman, A Universal Operator Growth Hypothesis, *Phys. Rev. X* **9**, 041017 (2019).
- [5] J. Maldacena, S. H. Shenker, and D. Stanford, A bound on chaos, *J. High Energy Phys.* **2016** (8), 1.
- [6] H. Tang, Operator Krylov complexity in random matrix theory, arXiv [10.48550/arXiv.2312.17416](https://arxiv.org/abs/10.48550/arXiv.2312.17416) (2023), [2312.17416](https://arxiv.org/abs/2312.17416).
- [7] J. L. F. Barbón, E. Rabinovici, R. Shir, and R. Sinha, On the evolution of operator complexity beyond scrambling, *J. High Energy Phys.* **2019** (10), 1.
- [8] E. Rabinovici, A. Sánchez-Garrido, R. Shir, and J. Sonner, Krylov complexity from integrability to chaos, *J. High Energy Phys.* **2022** (7), 1.
- [9] L. Fleishman and D. C. Licciardello, Fluctuations and localization in one dimension, *J. Phys. C: Solid State Phys.* **10**, L125 (1977).
- [10] J. Maldacena and D. Stanford, Remarks on the Sachdev-Ye-Kitaev model, *Phys. Rev. D* **94**, 106002 (2016).
- [11] D. K. Nandy, T. Čadež, B. Dietz, A. Andreanov, and D. Rosa, Delayed thermalization in the mass-deformed Sachdev-Ye-Kitaev model, *Phys. Rev. B* **106**, 245147 (2022).
- [12] J. S. Cotler, G. Gur-Ari, M. Hanada, J. Polchinski, P. Saad, S. H. Shenker, D. Stanford, A. Streicher, and M. Tezuka, Black holes and random matrices, *J. High Energy Phys.* **2017** (5), 1.
- [13] N. Pancotti, G. Giudice, J. I. Cirac, J. P. Garrahan, and M. C. Bañuls, Quantum East Model: Localization, Nonthermal Eigenstates, and Slow Dynamics, *Phys. Rev. X* **10**, 021051 (2020).